



저작자표시-비영리-변경금지 2.0 대한민국

이용자는 아래의 조건을 따르는 경우에 한하여 자유롭게

- 이 저작물을 복제, 배포, 전송, 전시, 공연 및 방송할 수 있습니다.

다음과 같은 조건을 따라야 합니다:



저작자표시. 귀하는 원저작자를 표시하여야 합니다.



비영리. 귀하는 이 저작물을 영리 목적으로 이용할 수 없습니다.



변경금지. 귀하는 이 저작물을 개작, 변형 또는 가공할 수 없습니다.

- 귀하는, 이 저작물의 재이용이나 배포의 경우, 이 저작물에 적용된 이용허락조건을 명확하게 나타내어야 합니다.
- 저작권자로부터 별도의 허가를 받으면 이러한 조건들은 적용되지 않습니다.

저작권법에 따른 이용자의 권리는 위의 내용에 의하여 영향을 받지 않습니다.

이것은 [이용허락규약\(Legal Code\)](#)을 이해하기 쉽게 요약한 것입니다.

[Disclaimer](#)

碩士學位論文

Multi-Nozzle Electrohydrodynamic Inkjet Printing
for Fabrication of Electrically Functional Micro-
Structures

濟州大學校大學院

메카트로닉스工學科

알샤드 칸(艾爾沙德·汗)

2011 年 06 月

Multi-Nozzle Electrohydrodynamic Inkjet Printing for Fabrication of Electrically Functional Micro- Structures

指導教授 崔勁賢

알샤드 칸(艾爾沙德·汗)

이論文을 工學碩士學位論文으로 提出함

2011 年 06 月

알샤드 칸 (艾爾沙德·汗)의 工學碩士學位論文을 認准함

審査委員長

조경호

委員

강채영

委員

최정현

濟州大學校大學院

2011 年 06 月

Multi-Nozzle Electrohydrodynamic Inkjet Printing for Fabrication of Electrically Functional Micro- Structures

Arshad Khan

(Supervised by Prof. Kyung-Hyun Choi, Jeju National University)

A thesis submitted in partial fulfillment of the requirement for the degree of Master
of Science

2011. 06

This thesis has been examined and approved

.....
Thesis Committee Chair, Kyung-Ho Cho,


.....
Prof. of Jeju National University

.....
Thesis Committee Member, Chul-Ung Kang,


.....
Prof. of Jeju National University

.....
Thesis Director, Kyung-Hyun Choi,


.....
Prof. of Jeju National University

Department of Mechatronics Engineering
GRDUATE SCHOOL
JEJU NATIONAL UNIVERSITY



Dedicated to My Grandmother

Acknowledgements

By the name of Almighty Allah, the most merciful, the most beneficent. I would like to present my humble gratitude in front of Allah Almighty, Who enabled me to accomplish the dignified cause of education and learning, and I would pray Him that He makes me able to utilize my knowledge and edification for the betterment of humanity and its development.

I am heartily thankful to my supervisor Prof. Kyung Hyun Choi, whom encouragement, guidance and support from the initial to the final level enabled me to develop an understanding of the subject. This thesis would not have been possible without his keen interest and valuable support. Also I would like to pay my thanks to Dr. Dong Soo Kim for his full support to access KIMM (Korean Institute of Machinery and Materials) facilities for results analysis.

I extend my thanks to all my lab colleagues and co-workers (Khalid Rahman, Nauman Malik, Saleem Khan, Adnan Ali, Ahsan Rahman, Awais Naeem, Ganesh Thangaraj, Sridharan, Maria Mustafa, Navaneethan, Lee Kyung-Hyun, Ko Jeong-beom, Dang Hyun-Hoo, Kim Hyung-Chan, Park Jae-Hee, Yoo Ji-Youne) for the fruitful discussions and helping me out through all the ups and downs of my stay here in Korea. They have been great resources of encouragement and insight into many topics as well as great sounding board for my bizarre ideas. The lovely memories I have with these guys will always be cherished. I would like to especially mention Khalid Rahman and Nauman Malik for their continuous and invaluable support.

My deepest gratitude goes to my parents for their understanding and spiritual/financial supports. None of my endeavors would be possible without them. Especially, I pay my homage to my grandmother who passed away during my master studies.

Lastly, I offer my regards and blessings to all of those who supported me in any respect during the completion of the project.

Table of Contents

List of Figures	iv
List of Tables	vii
요약	viii
Abstract	ix
1. Introduction	1
1.1 Background and Motivation	1
1.2 Competing Technologies	3
1.3 Thesis Overview	4
2. Fundamentals of EHD Inkjet Printing Process	5
2.1 Working Principle	5
2.2 Forces Acting on Liquid Meniscus	7
2.3 Governing Equations for Electrohydrodynamic Flow	9
2.4 Major Modes of EHD Inkjet Printing	11
2.4.1 Continuous Mode	12
2.4.2 Drop-on-Demand Mode	12
2.5 Applications of EHD Inkjet Printing	13
3. Cross-Talk in Multi-Nozzle EHD inkjet Printing	14
3.1 Numerical Simulation	15
3.2 End Effect	19
3.3 Effects of Process Parameters on Cross-Talk	20
3.3.1 Flow Rate	20
3.3.2 Applied Voltage	21

3.3.3 Nozzle-to-Nozzle Distance	22
3.3.4 Nozzles Array Configuration	23
3.3.5 Material Composition of the Printing Nozzle	25
3.3.6 Nozzle Diameter	26
4. Experimental Methods	27
4.1 Inks Used	27
4.1.1 Silver Colloidal Solution.....	28
4.1.2 Copper Colloidal Solution	29
4.1.3 Organo-Metallic Ink.....	30
4.2 Development of Multi-Nozzle EHD Inkjet Printing Head	31
4.2.1 3ND Multi-Nozzle EHD Inkjet Printing Head.....	31
4.2.2 5ND Multi-Nozzle EHD Inkjet Printing Head.....	38
4.2.3 5NI Multi-Nozzle EHD Inkjet Printing Head	39
4.3 Experimental Set-Up.....	41
5. Printed Results and Characterization	45
5.1 Results of 3ND Multi-Nozzle EHD Inkjet Printing Head	45
5.1.1 Axisymmetric Micro-jet Generation	45
5.1.2 Printed Results on Glass Substrate.....	46
5.1.3 X-ray diffraction Analysis of the Printed Lines	47
5.1.4 Scanning Electron Microscopy of the Printed Lines.....	48
5.1.5 Electrical Characterization of the Printed Lines	49
5.2 Results of 5ND Multi-Nozzle EHD Inkjet Printing Head	51
5.2.1 Axisymmetric Micro-jet Generation	52
5.2.2 Printed Results on Glass Substrate.....	52
5.2.3 X-ray diffraction Analysis of the Printed Lines	53
5.2.4 Scanning Electron Microscopy of the Printed Lines.....	54

5.2.5 Electrical Characterization of the Printed Lines	55
5.3 Results of 5NI Multi-Nozzle EHD Inkjet Printing Head	57
5.3.1 Printed Results on Glass Substrate.....	57
5.3.2 Scanning Electron Microscopy of the Printed Lines.....	58
5.3.3 Electrical Characterization of the Printed Lines	59
Conclusions.....	60
References.....	61
List of Publications	a
Appendices.....	i

List of Figures

Figure 1 Methodology of EHD inkjet printing process (a) Schematic illustration of EHD inkjet printing technique (b) When no electric potential is applied i.e. liquid is driven by pressure forces only (c) Taylor cone with a continuous thin jet emanating from its tip (d) Taylor cone with a small droplet ejecting from its tip	7
Figure 2 Stress acting on the liquid meniscus after the application of an electric potential	8
Figure 3 Schematic of FEA model used for electric field simulation.....	16
Figure 4 Electric field simulation results of linear array of nozzles at applied voltage of 8 kV and having nozzle-to-nozzle distance of 5mm	17
Figure 5 Electric field simulation results of triangular array of nozzles at applied voltage of 8 kV and having nozzle-to-nozzle distance of 5mm	17
Figure 6 Jetting image of triangular array multi-nozzle EHD inkjet printing head, showing deflection of the meniscus at the peripheral nozzles.....	20
Figure 7 Jetting angles at boundary nozzles of a triangular array of nozzles, 3mm nozzle-to-nozzle gap and at constant applied voltage of 6kV	21
Figure 8 Jetting angles at boundary nozzles of a triangular array of nozzles, 3mm nozzle-to- nozzle gap and at constant flow rate of 0.0026 ml/min	22
Figure 9 Jetting angles at boundary nozzles of a triangular array of nozzles, 5mm nozzle-to- nozzle gap and at constant flow rate of 0.0026 ml/min	23
Figure 10 Comparison of jetting angles at boundary nozzles of linear array multi-nozzle EHD inkjet printing head and triangular array multi-nozzle EHD inkjet printing head (a) 3mm nozzle-to-nozzle gap, at different applied voltages and constant flow rate of 0.026 ml/min (b) 5mm nozzle-to-nozzle gap, at different applied voltages and constant flow rate of 0.0013 ml/min.....	25

Figure 11 (a) of the FEA model used for electric field simulation (b) Simulation in COMSOL 3.5a of the electric field lines	34
Figure 12 Schematic illustration of the 3ND multi-nozzle EHD inkjet printing head fabrication process: (a) Simplified fabrication steps of mold preparation (detailed drawing is shown in appendix A) (b) Resulted PDMS holder having L-shaped channels for ink supply and claspings of glass capillaries (c) Complete multi-nozzle EHD inkjet printing head	37
Figure 13 Photograph of the 3ND multi-nozzle EHD inkjet printing head	37
Figure 14 Schematic illustration of the multi-nozzle EHD inkjet printing head fabrication process: (a) Simplified fabrication steps of mold preparation (detailed drawing is shown in appendix B) (b) PDMS holder having L-shaped channels for ink supply (c) Complete multi-nozzle EHD inkjet printing head....	39
Figure 15 Schematic illustrations of 5NI multi-nozzle EHD inkjet printing head (a) Holder for the nozzle and the ground ring (b) cross-sectional view of the holder (c) complete printing head	40
Figure 16 Photograph of 5NI multi-nozzle EHD inkjet printing head (a) without integrated ground ring (b) with integrated ground ring	41
Figure 17 Schematic illustrations of experimental setups using (a) 3ND multi-nozzle EHD inkjet printing head (b) 5ND multi-nozzle EHD inkjet printing head (c) 5NI multi-nozzle EHD inkjet printing head.....	43
Figure 18 Photograph of EHD inkjet printing rig used for experiments.....	44
Figure 19 Photographs of axisymmetric liquid menisci established at the nozzle tips of 3ND multi-nozzle EHD inkjet printing head	46
Figure 20 High-zoom static camera and optical microscope image of continuous silver lines printed on glass substrate by 3ND multi-nozzle EHD inkjet printing technique. The bottom inset shows the average line width of 140 μ m	47
Figure 21 X-ray diffraction (XRD) spectrum of the printed line	48
Figure 22 SEM image of continuous silver track deposited by 3ND multi-nozzle EHD inkjet printing head. The bottom inset shows the three-dimensionally interconnected silver nanoparticles.....	49

Figure 23 (a) linearly Ohmic I–V curve of the printed lines (b) AFM image and cross– sectional profile of a typical silver line printed by multi-nozzle EHD inkjet printing process	51
Figure 24 High speed camera images of axisymmetric cone-jets formed at the nozzles tips of 5ND multi-nozzle EHD inkjet print head.....	52
Figure 25 Optical microscope images of continuous copper tracks printed simultaneously onto glass substrate using 5ND multi-nozzle EHD inkjet printing head	53
Figure 26 XRD Pattern of the multi-nozzle EHD inkjet Printed copper film, sintered at 230 °C under inert atmosphere.....	54
Figure 27 SEM image of copper track deposited by 5ND multi-nozzle EHD inkjet printing head. The bottom inset shows that copper nanoparticles are three-dimensionally interconnected with each other....	55
Figure 28(a) Linearly Ohmic I-V curve of the printed copper conductive lines (b) Cross-sectional image and AFM 3D topographical view (100 μm × 100 μm) of a typical copper track on a glass substrate, printed by 5ND multi-nozzle EHD inkjet printing head.....	56
Figure 29 Optical microscope images of continuous silver tracks printed simultaneously onto glass substrate using 5ND multi-nozzle EHD inkjet printing head	57
Figure 30 SEM image of silver track deposited by 5NI multi-nozzle EHD inkjet printing head. The bottom insets show densely packed crystallites.....	58
Figure 31 Cross-sectional image and AFM 3D topographical view (100 μm × 100 μm) of a typical silver line on a glass substrate, printed by 5NI multi-nozzle EHD inkjet printing head.....	59

List of Tables

Table 1 Types of nozzles array configurations tested for electric field simulations	16
Table 2 Simulated Electric field values (kV/m) around the tip of each nozzle of linear array of nozzles at different applied voltages and having nozzle-to-nozzle gap of 5 mm	18
Table 3 Simulated electric field values (kV/m) around the tip of each nozzle of triangular array of nozzles at different applied voltages and having nozzle-to-nozzle gap of 5 mm	18
Table 4 Simulated Electric field values (kV/m) around the tip of each nozzle of linear array of nozzles at different applied voltages and having nozzle-to-nozzle gap of 3 mm	19
Table 5 Simulated Electric field values (kV/m) around the tip of each nozzle of triangular array of nozzles at different applied voltages and having nozzle-to-nozzle gap of 3 mm.....	19
Table 6 Properties of silver colloidal solution used for experiments	28
Table 7 Properties of copper colloidal solution used for experiments	30
Table 8 Properties of silver organo-metallic ink used for experiments.....	30
Table 9 Details of electric field simulation parameters used for analysis.	34
Table 10 Simulated Electric field (kV/m) values around the meniscus of each nozzle on different points at an applied voltage of 3.5 kV and nozzle-to-nozzle gap of 2.5 mm.....	35
Table 11 Simulated Electric field (kV/m) values around the meniscus of each nozzle on different points at an applied voltage of 3.5 kV and nozzle-to-nozzle gap of 3 mm.....	35

요약

Electrohydrodynamic (EHD) 잉크젯 프린팅 공정은 노즐 오리피스에 비해 매우 작은 제트나 방울 생성의 독특한 특징 때문에 압전 및 열 기반의 잉크젯 인쇄 기술에 있어 유망한 대안으로 여겨진다.

비록 EHD 잉크젯 인쇄 공정에 의한 직접적인 증착은 미세한 패터닝에 있어 다양한 장점을 제공하지만, EHD 잉크젯 인쇄의 낮은 원료처리량 즉, 낮은 생산 속도는 전자 산업에 있어서 가능한 광범위한 적용에 방해가 되는 심각한 단점이 있다.

EHD 잉크젯 인쇄 공정의 낮은 생산 속도의 한계를 극복하고 낮은 가격의 전자 미세 구조물을 가공하기 위하여 이 논문은 다중 노즐 EHD 잉크젯 프린팅 공정을 사용하여 콜로이드 솔루션의 직접 인쇄를 제시한다. 전기 충전된 이웃 제트 사이의 상호 작용(cross-talk)에 대한 멀티 노즐 EHD 잉크젯 인쇄 공정에서 일반적인 배경을 제공하는 수치 및 실험적인 조사이다.

노즐과 실험 조건 사이의 거리가 전기 충전된 이웃 제트 사이의 상호 작용(cross-talk)을 방지하기 위해 최적화되었다.

멀티 노즐 EHD 잉크젯 인쇄 헤드의 세 가지 다른 종류를 가공하고 동시에 유리 기판에 전기 전도성 마이크로 트랙을 인쇄하는 것에 의한 성공적인 실험이 이루어졌다.

인쇄된 트랙은 광학 현미경, 전자 현미경 (SEM)에 스캐닝, X - 선 회절 (XRD), 4 포인트 프로브를 등 다양한 특성화 도구를 사용하여 모두 물리적 및 전기적으로 분석했다.

트랙은 실버 콜로이드 용액과 구리 콜로이드 용액에 대해 각각 $5.05 \times 10^{-8} \Omega.m$, $9.20 \mu\Omega.cm$ 의 전기 저항을 보여준다. 이러한 전도성 마이크로 트랙은 마이크로 전자 구조 및 장치의 제조산업에 있어서 다중 노즐 EHD 잉크젯 인쇄 공정의 가능성을 보여줍니다.

Abstract

Electrohydrodynamic (EHD) inkjet printing process is considered to be a promising alternative to piezoelectric and thermal based inkjet printing techniques because of its unique feature of generating very small jet or droplets as compared to the nozzle orifice. Though direct deposition by EHD inkjet printing process offers various advantages in fine patterning, however the low production speed i.e. low throughput of EHD inkjet printing is a severe drawback that has hampered its possible widespread applications in electronic industry. To overcome the limitation of low production speed of EHD inkjet printing process and to fabricate low cost electronic microstructures, this dissertation presents the direct printing of colloidal solutions using multi-nozzle EHD inkjet printing process. Interaction (cross-talk) between the electrically charged neighboring jets is investigated both numerically and experimentally to provide the reader a general background in multi-nozzle EHD inkjet printing process. Distance between the nozzles and experimental conditions were optimized to prevent the cross-talk between electrically charged neighboring jets. Three different types of multi-nozzle EHD inkjet printing heads were fabricated and successfully tested by simultaneously printing electrically conductive micro tracks onto the glass substrate. The printed tracks were analyzed both physically and electrically by using different characterization tools such as optical microscopy, scanning electron microscopy (SEM), atomic force microscopy (AFM), X-ray diffraction (XRD) and four-point probe. The tracks show electrical resistivity of $5.05 \times 10^{-8} \Omega.m$, $9.20 \times 10^{-8} \Omega.m$ and $6.47 \times 10^{-8} \Omega.m$ for silver colloidal solution and copper colloidal solution and silver organo-metallic respectively. These electrically conductive micro-tracks demonstrate the feasibility of multi-nozzle EHD inkjet printing process in industrial fabrication of microelectronic structures and devices.

1. Introduction

1.1 Background and Motivation

Development of Inkjet printing technology for rapid prototyping of electronic microstructures or patterns has attracted much attention in recent years because of its low cost, non contact mask-free deposition of wide-range of materials on variety of substrates [1, 2]. Number of inkjet printers based on different actuation mechanisms like thermal, piezoelectric and aerosols are widely used in electronic industry [3]. To maintain high printing throughput in these printers, multi-nozzle printing process has been investigated by many researchers over the years. Multi-nozzle piezoelectric inkjet printing heads typically consist of tens, hundreds or even thousands [4] of separate nozzles were fabricated and successfully used for microelectronic device fabrication. Wang et al. fabricated a multi-nozzle thermal inkjet printing head by silicon micromachining technology using a dense array of thermal bubble inkjet devices made on a single silicon wafer [5]. Optomec, Inc. had developed a commercially available multi-nozzle aerosol inkjet printing head in order to meet the needs of photovoltaic manufacturers. The printing head is closely coupled with a series of atomizers to insure efficient distribution of inks through the print head manifold [6].

The above inkjet printers are already commercialized, however due to various intrinsic problems of nozzle blockage and overheating of organic materials in these existing printing devices, a new direct printing process based on electrohydrodynamic (EHD) atomization is the focal research topic for many industrial and academic researchers [7]. EHD inkjet printing process is considered to be a promising alternative to piezoelectric and thermal based inkjet printing techniques because of its unique feature of generating very small jet or droplets as

compared to the nozzle orifice [8]. Several researchers demonstrated the feasibility of EHD inkjet printing process in manufacturing of microelectronic devices by direct fabrication of high-resolution printed metal interconnects electrodes [8], collectors for printed solar cells [9] and electrodes for thin film transistors [10, 11] with critical dimensions much smaller than that of the printing nozzle.

Though direct deposition by EHD inkjet printing process offers various advantages in fine patterning, however the low production speed i.e. low throughput of EHD printing is a severe drawback that has hampered its possible widespread applications in electronic industry. Recently, Zhouping et al. presented a comprehensive review about conventional inkjet printing technology and EHD inkjet printing technology for flexible electronics applications highlighting the production speed as a major limitation of EHD inkjet printing technology [12]. In order to surmount this drawback and attain high production efficiency EHD inkjet printing process for industrial production of printed displays, PCBs, printed TFTs and printed solar cells, a multi-nozzle EHD inkjet printing process has been primarily investigated by few scientists [13-15]. Most of these studies have focused on making stable cone-jet and reducing the positioning error of the ejected jet. However due to the cross-talk between the electrically charged neighboring jets, a well controlled and reproducible multi-nozzle EHD inkjet printing process has not been reported in the literature.

In this thesis, cross-talk between the electrically charged neighboring jets is first investigated both numerically and experimentally to obtain a more complete picture of multi-nozzle EHD inkjet printing process. The wealth of information obtained from such investigation is expected to complement and to some extent help the reader to gain a more complete understanding of this complex multi-nozzle EHD inkjet printing process. Then, as a result of

these investigations, the distance between the nozzles and experimental conditions were optimized to prevent the cross-talk between electrically charged neighboring jets. Using this optimized nozzle-to-nozzle distance, three different types of multi-nozzle EHD inkjet printing heads were fabricated and successfully tested by simultaneously printing electrically conductive micro tracks onto the glass substrate. The printed tracks were analyzed both physically and electrically by using different characterization tools such as optical microscopy, scanning electron microscopy (SEM), atomic force microscopy (AFM), X-ray diffraction (XRD) and four point probe. These conductive micro-tracks demonstrate the feasibility of multi-nozzle EHD inkjet printing process in industrial fabrication of microelectronic structures and devices.

1.2 Competing Technologies

There are currently several direct writing technologies which are in competition with electrohydrodynamic inkjet printing technology. In general, they can be divided into two main categories based on their approaches. One is the “direct deposition” while the other is “pattern-a-pool”. The first category involves direct transfer of patterned materials from nozzle to a substrate. Materials are dispensed dropwise, extruded as a continuous filament, or transferred in a ‘dip-pen’ fashion. Common technologies in this category include conventional inkjet printing, micro-pen, fused deposition method (FDM), dip-pen nanolithography (DPN), and 3D printing. While the pattern-a-pool category starts with a thin layer of ceramic powder or slurry bed, and then selectively bind the powder or slurry together by a laser or binder solution. Typical examples include stereo-lithography (SLA) as well as 3DP mentioned previously [7].

1.3 Thesis Overview

This dissertation focuses on multi-nozzle EHD inkjet printing process in detail. Chapter 2 concentrates on the fundamentals of EHD inkjet printing process and its applications. In order to provide the reader a general background in multi-nozzle EHD inkjet printing process, chapter 3 presents the numerical and experimental investigations of the cross-talk between the electrically charged neighboring jets. Chapter 4 describes the details of multi-nozzle EHD inkjet printing head development, material used, experimental setup and instrumentation. A customized multi-nozzle EHD inkjet printing rig has been developed. For the first time, a multi-channel pump and a voltage distributor are used for individual ink supply and voltage supply to each nozzle respectively. Printed results of the multi-nozzle electrohydrodynamic (EHD) inkjet printing heads are reported in chapter 5. The printed tracks are analyzed both physically and electrically by using different characterization tools such as optical microscopy, scanning electron microscopy (SEM), atomic force microscopy (AFM), X-ray diffraction (XRD) and four point probe. Finally, a brief summary of the key accomplishments has been presented.

2. Fundamentals of EHD Inkjet Printing Process

Electrohydrodynamic (EHD) inkjet printing pulls the fluids rather than pushes them like conventional inkjet printing processes; therefore it generates very small jet or droplets as compared to the nozzle orifice [8] and offers some unique features, such as allowing submicron resolution [10], and easy processing of particulate or polymer solutions without clogging the nozzle. In other words the resolution is not limited by the nozzle diameter [16]. Using coarser nozzles prevents them from clogging, however at the same time the droplets/jet can be of sub-micrometer size [17].

In this chapter, the critical findings are summarized to provide the reader a general background in EHD inkjet printing. First in section 2.1, the working principle of EHD inkjet is defined. Based on the static balance between surface tension and electrical stress acting on the meniscus, section 2.2 discusses the forces acting on the liquid surface. In section 2.3, the governing equations for electrohydrodynamic flow and for stable cone-jet formation are presented. Then in section 2.4, the two major modes of EHD printing are briefly discussed. Finally in section 2.5, some important applications of EHD inkjet printing are presented.

2.1 Working Principle

Electrohydrodynamic inkjet printing uses electric fields, rather than thermal or acoustic energy for liquid flow generation. Figure 1a shows a schematic illustration of EHD inkjet printing technique. When a liquid i.e. ink is supplied to a nozzle without applying electric potential, a hemispherical meniscus pendent at the nozzle tip is formed by the surface tension at

the interface between the liquid and air (Figure 1b), because droplet stays spherical as the surface tension tends to minimize the interfacial energy. To deform this hemispherical meniscus to a cone, certain amount of electric potential is required. As the electric potential difference is applied between the nozzle and the ground electrode, Electric charges having the same polarities accumulate at the surface of the liquid meniscus originating Maxwell electrical stress which eventually causes the hemispherical meniscus to deform into a liquid cone (known as Taylor cone [18]). With the increase in the electric field strength, the pinnacle of Taylor cone ejects a small liquid jet (Figure 1c) or droplet (Figure 1d), depending on the type of the applied electric potential.

This ejection of very small jet/droplet compared to the nozzle orifice is the main advantage of EHD inkjet printing technique. The emitted jet diameter can be two orders of magnitude smaller than that of the printing nozzle [7]. Therefore, it enables printing at much finer resolution without miniaturizing the printing nozzle, which is particularly useful in printing highly viscous colloidal solutions or viscous polymeric fluids [19].

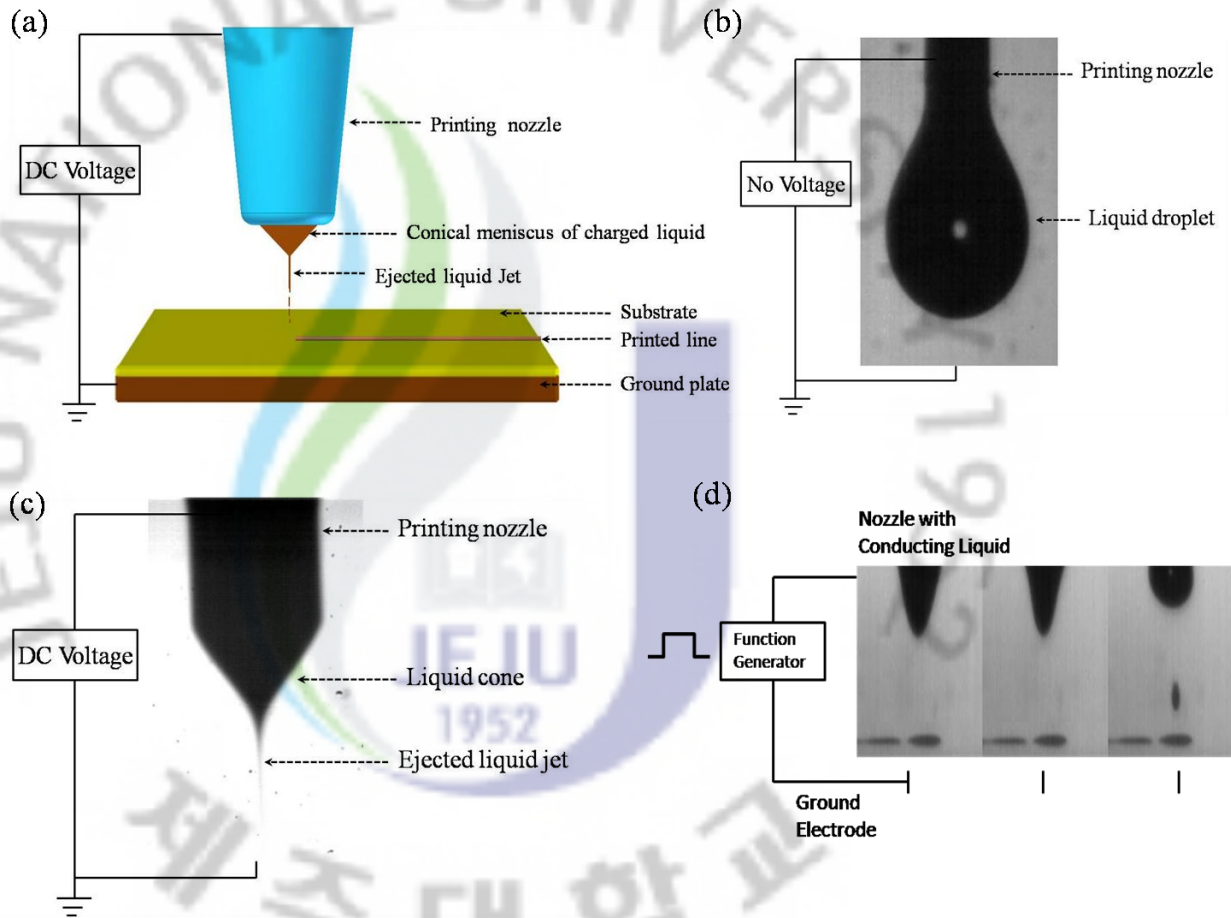


Figure 1 Methodology of EHD inkjet printing process (a) Schematic illustration of EHD inkjet printing technique (b) When no electric potential is applied i.e. liquid is driven by pressure forces only (c) Taylor cone with a continuous thin jet emanating from its tip (d) Taylor cone with a small droplet ejecting from its tip

2.2 Forces Acting on Liquid Meniscus

When electric potential is applied, the surface of the liquid meniscus (Figure 2) is mainly subjected to surface tension (σ_s), hydrostatic pressure (σ_h) and electrostatic pressure (σ_e). If the liquid is considered to be a pure conductor, then the electric field will be perpendicular to the liquid surface and no tangential stress component will be acting on the liquid surface. The liquid bulk will be neutral and the free charges will be confined in a very thin layer. This situation can be summarized in the following equations [20].

$$\sigma_h + \sigma_e + \sigma_s = 0 \quad (2.1)$$

$$\sigma_h = \rho g \Delta h \quad (2.2)$$

$$\sigma_e = \frac{E_n^2}{2\epsilon_r} \quad (2.3)$$

Where ρ is the density of liquid, g is the acceleration due to gravity, Δh is the liquid level difference between the container and the free end of the nozzle, ϵ_r is the permittivity of the liquid, and E_n is the electric field strength normal to the liquid surface. Since the liquid i.e. ink is not a perfect conductor therefore the resultant electric polarization stress on the liquid surface has two components i.e. normal component and tangential component. The direction of these components is shown in Figure 2. The normal electric stress destabilizes the jet while the tangential electric stress will move liquid from the meniscus surface to the apex of the meniscus to form a jet. When the tangential stress is strong enough, a stable cone-jet is formed [21].

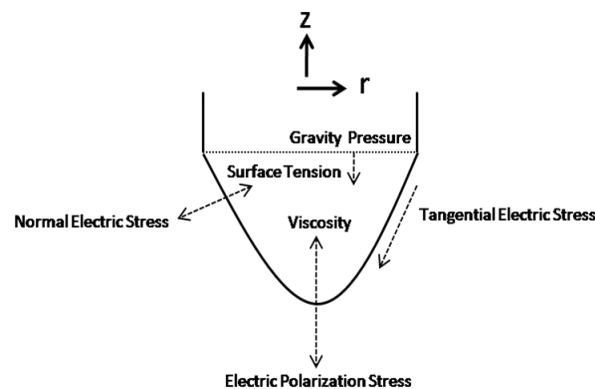


Figure 2 Stress acting on the liquid meniscus after the application of an electric potential

2.3 Governing Equations for Electrohydrodynamic Flow

Electrohydrodynamic atomization (EHDA) system consists of two phases i.e. the liquid phase and the gas phase (ambient air). In addition, the multiphase flow is coupled with the applied electric potential field and electric charging on the interface. Assuming the system to be isothermal and considering both liquid and gas phases incompressible. Then, the mass conservation of the whole domain, which consists of both the gas phase and the liquid phase can be expressed as,

$$\nabla \cdot \bar{u} = 0 \quad (2.4)$$

Where \bar{u} is the velocity of the fluid. To take into account the surface tension on liquid-gas interface (F_{ST}), the electrical stresses (F_{ES}) and gravitational force, the Navier-Stokes equation would need to include the additional terms for these forces and can be expressed as,

$$\frac{\partial \rho \bar{u}}{\partial t} + \nabla \cdot \rho \bar{u} \bar{u} = -\nabla p + \nabla [\mu (\nabla \bar{u} + \nabla \bar{u}^T)] + (\rho - \rho_g) \bar{g} + \bar{F}_{ST} + \bar{F}_{ES} \quad (2.5)$$

Where p is the pressure, μ is the viscosity of the fluid, \bar{g} is the gravitational acceleration. Subscript g refers to the gas phase. The surface tension force on the liquid-gas interface can be calculated as follows,

$$\bar{F}_{ST} = \int_{\Gamma} \sigma \kappa \bar{n} \delta(\bar{x} - \bar{x}_f) ds_f \quad (2.6)$$

Where σ is the surface tension, κ is the curvature of the interface; Subscript f refers to the front or interface. $\delta(\bar{x} - \bar{x}_f)$ is a dirac-delta function, which is used to impose the surface tension force acting on the perimeter of the control volume where the interface is located.

The electrical volume stress can be calculated by taking the divergence of the Maxwell stress tensor (σ^M) while assuming that the fluid is incompressible [22].

$$\vec{F}_{ES} = \nabla \cdot \sigma^M = -\frac{1}{2} \vec{E} \cdot \vec{E} \nabla \varepsilon + q^v \vec{E} \quad (2.7)$$

Where \vec{E} is electric field, and q^v is the volume charge density near the interface. The first term on the right of equation (2.7) is due to the polarization stress, and it acts in the normal direction of the interface as a result of the term $\nabla \varepsilon$. The second term is due to the interaction of the electric charges with the electric field and acts in the direction of the electrical field. Since it was assumed that the electric charges are located on the interface therefore both the polarization electrical stress and the charge field interaction electrical stress would thus be exerted on the interface.

The distribution of electric charge can be approximated by first considering two inter-related parameters, the electrical relaxation time of the system and the Debye length. The electrical relaxation time [23] is used to define the charge relaxation time (τ^E) in the electrohydrodynamic system. It is defined as the ratio of the electrical permittivity (ε) over the electrical conductivity (K),

$$\tau^E = \frac{\varepsilon}{K} \quad (2.8)$$

The Debye length is related to the thickness of the electric charge boundary layer, where the electric charges will be located when it is distributed on the surface of an electrohydrodynamic system [24]. The Debye Length (λ) can be defined as,

$$\lambda = \sqrt{D\tau^E} \quad (2.9)$$

Note that the molecular diffusivity (D) of the charge species and the electrical permittivity of the system have a positive effect on increasing the Debye length, while increasing the electrical conductivity decreases the Debye length.

For electrohydrodynamic atomization to take place, the charge relaxation-time constant must be much smaller than the hydrodynamic relaxation-time constant [25]. This establishes the inequality,

$$\frac{\varepsilon}{K} \ll \frac{\eta r_0}{\sigma} \quad (2.10)$$

Where η is the viscosity of the liquid, while r_0 represents the outer radius of the nozzle.

The electric field required to establish a Taylor cone at the nozzle tip opposite to a flat plate (as a counter electrode) in a single nozzle set up is given by the following equation [26],

$$\bar{E} = \left(\frac{2\sigma \cos \theta}{\varepsilon_0 r_0} \right)^{1/2} \quad (2.11)$$

Where ε_0 is the permittivity of free space and θ is the Taylor cone angle usually taken as 49.3° [18]. Similarly, potential difference across the electrode required to reach the above electric field strength is given by [26],

$$V_c = 0.667 \left(2\sigma r_0 \cos \theta / \varepsilon_0 \right)^{1/2} \ln \left(\frac{4h}{r_0} \right) \quad (2.12)$$

Where V_c is the onset electric potential, and h is the spacing between the counter electrodes.

2.4 Major Modes of EHD Inkjet Printing

There are varieties of functioning modes of EHD atomization [27, 28]. However, in the following subsections, the two major modes of printing i.e. continuous (Figure 1c) and drop-on-demand (Figure 1d) are briefly described, as only these modes of printing are used in the present study.

2.4.1 Continuous Mode

Continuous EHD inkjet printing (Figure 1c) is the most suitable direct writing approach of colloidal solutions for low resolution patterning. The main advantages of continuous inkjet are its speed and the high velocity of the jet that enables it to travel a larger distance to the substrate. The fact that there is a continuous flow of ink through the nozzles minimizes the risk of clogging them. Another advantage of continuous EHD inkjet printing is that the scattering masses is significantly less for the submicron resolution printing in continuous mode than that of drop-on-demand mode. Furthermore, since continuous mode only form continuous lines and not a series of dots, therefore the use of continuous mode eliminates the requirement of overlapping of successive ink droplets to produce a continuous line [7].

2.4.2 Drop-on-Demand Mode

In EHD drop-on-demand printing mode (Figure 1d), a pulsed voltage is applied to the capillary for liquid charging instead of continuous dc voltage which causes the meniscus to deform into a cone and forms a droplet rather than continuous jet. The reason for this strategy is that the normal electric stress (Figure 2) is likely to produce a drop-on-demand printing also known as dripping mode while the tangential electric stress will move the liquid/ink from the meniscus surface to the apex of the meniscus to form a tiny jet. When the tangential electric stress is strong enough, a cone-jet known as continuous mode of printing is formed. Therefore to avoid the intensive tangential stress i.e. continuous mode of printing, simple pulse voltage or pulse voltage superimposed on dc voltage instead of simple dc voltage is applied for drop-on-demand printing [29].

2.5 Applications of EHD Inkjet Printing

Since EHD inkjet printing process has great potential to offer complex and high-resolution printing and is opening new routes to nanotechnology, therefore the proposed research is beneficial directly or indirectly for variety of scientific and industrial fields including material science, biotechnology (cell sorting, DNA micro array, DNA synthesis, drug discovery, Medical Therapeutics) manufacturing technology (optics, droplet based manufacturing, inkjet soldering, precision fluid deposition, thin film coatings, document security, integrated circuit manufacturing), printed microelectronics (printed solar cells, printed thin film transistors, organic light emitting diodes, printed batteries) etc.

3. Cross-Talk in Multi-Nozzle EHD inkjet Printing

Although direct deposition by electrohydrodynamic (EHD) inkjet printing process offers various advantages in manufacturing of microelectronic devices by direct fabrication of high-resolution printed metal interconnects electrodes [8], collectors for printed solar cells [9] and electrodes for thin film transistors [10, 11], however the low production speed i.e. low throughput of EHD inkjet printing is a severe drawback that has hampered its possible widespread applications in electronic industry. In order to surmount this drawback and attain high production efficiency EHD inkjet printing process for industrial production of printed displays, printed circuit boards (PCB), printed thin film transistors (TFT) and printed solar cells, a multi-nozzle EHD inkjet printing process has been primarily investigated by few scientists [13-15]. Most of these studies have focused on making stable cone-jet and reducing the positioning error of the ejected jet. However due to the interaction (cross-talk) between the electrically charged neighboring jets, a well controlled and reproducible multi-nozzle EHD inkjet printing process for simultaneous printing is very difficult to accomplish. This interaction breeds the asymmetric electric field around the meniscus of each nozzle, eventually destabilizing the resulted jets. A very limited data related to the analysis of the cross-talk between the neighboring jets is available in the literature [30].

In this chapter, cross-talk between the neighboring jets is investigated both numerically and experimentally to provide the reader a general background in multi-nozzle EHD inkjet printing process. First, in section 3.1 the details and findings of the numerical simulation are presented. Then, in section 3.2 the “end effect” which has been used as a measuring tool for the quantitative analysis of cross-talk between the neighboring jets is defined. Finally, in section 3.3

the effects of major parameters such as flow rate, applied voltage, nozzle-to-nozzle distance, nozzles array configuration, material composition of the printing nozzle, and nozzle diameter on the cross talk between the neighboring jets are enlisted.

3.1 Numerical Simulation

In order to understand the cross-talk between the neighboring jets in detail, electric field distribution around the tip of each nozzle was investigated. Electric field simulations were performed for the arrays consisting of three nozzles and having different array configurations (as shown in Table 1). Figure 3 shows the schematic of Finite Element Analysis (FEA) model used for the calculations of electric field distribution around the tip of the nozzles. The resulted electric field values for the case of 5mm nozzle-to-nozzle gap linear array of nozzles and triangular array of nozzles are shown in Figure 4 and Figure 5 respectively. In order to reveal the level of irregularity of electric field strength around the tip of each nozzle, the values of electric field strength on three different points A, B and C (as shown in Figure 3) were calculated at different applied voltages by solving the following governing equations:

$$\nabla \cdot (\varepsilon \nabla \phi) = q^v \quad (3.1)$$

$$\vec{E} = -\nabla \phi \quad (3.2)$$

Where \vec{E} indicates the electric field vector, ϕ is the applied electric potential, ε is the permittivity of ink and q^v is the electric charge density. These equations were solved by the finite element solver COMSOL Multiphysics 3.5a (Comsol Inc.) for three-dimensional geometries.

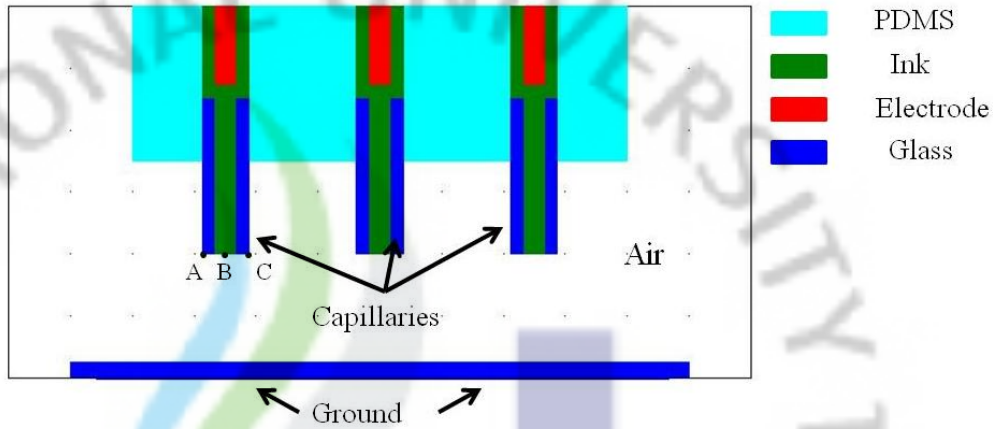


Figure 3 Schematic of FEA model used for electric field simulation

Table 1 Types of nozzles array configurations tested for electric field simulations

No.	Array Configuration	Nozzle-to-Nozzle Distance (mm)
1	Linear	5
2	Linear	3
3	Triangular	5
4	Triangular	3

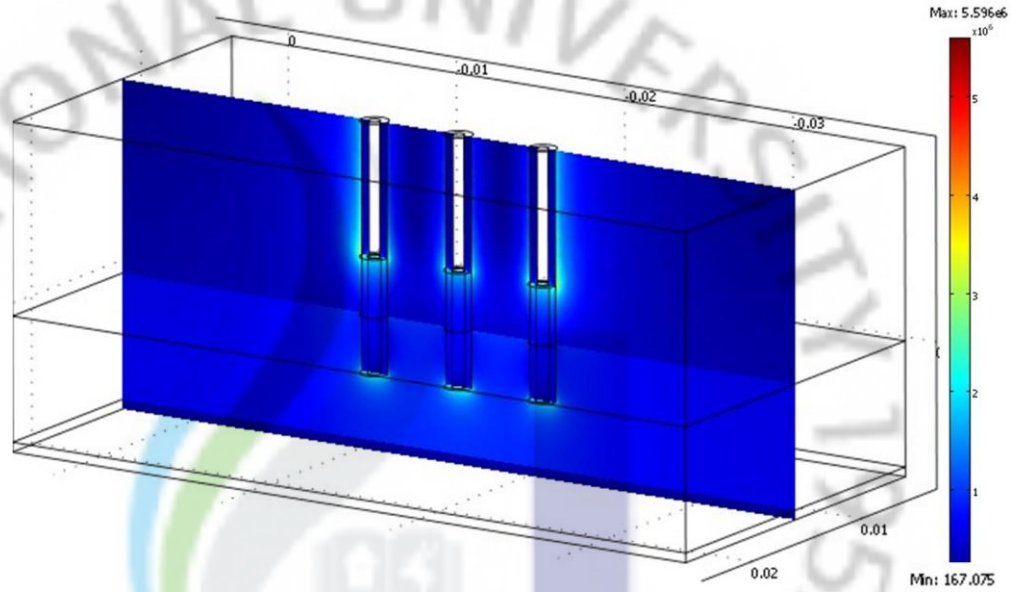


Figure 4 Electric field simulation results of linear array of nozzles at applied voltage of 8 kV and having nozzle-to-nozzle distance of 5mm

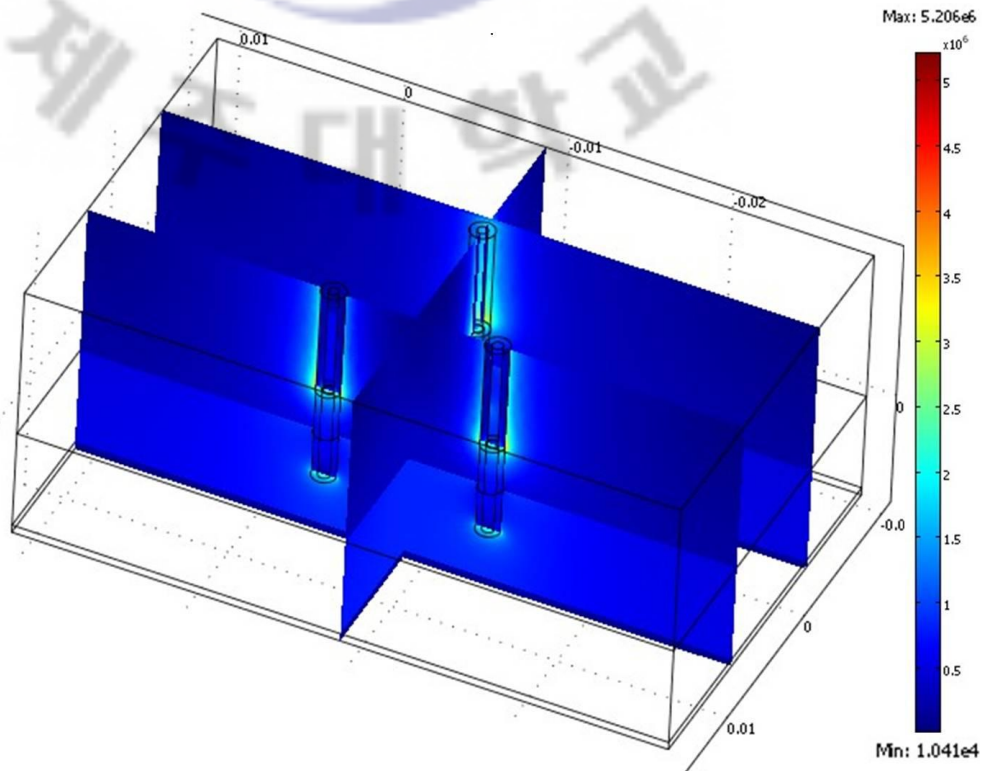


Figure 5 Electric field simulation results of triangular array of nozzles at applied voltage of 8 kV and having nozzle-to-nozzle distance of 5mm

The resulted electric field values around the tip of each nozzle at different applied voltages are also enlisted in Table 2 to Table 5. Table 2 presents the simulated electric field values at three different points (as shown in Figure 3) around the tip of each nozzle of a linear array having nozzle-to-nozzle gap of 5mm. Table 3 shows the simulated electric field values at the tip of each nozzle of the triangular array having 5 mm nozzle to nozzle gap for the same applied voltages and locations of the meniscus as that of the linear array of nozzles (Table 2). Similarly Table 4 and Table 5 show the electric field values around the tip of each nozzle (3 mm nozzle-to-nozzle gap) of the linear array of nozzles and the triangular array of nozzles respectively.

Table 2 Simulated Electric field values (kV/m) around the tip of each nozzle of linear array of nozzles at different applied voltages and having nozzle-to-nozzle gap of 5 mm

Applied Voltage (V)	Nozzle-1			Nozzle-2			Nozzle-3		
	A	B	C	A	B	C	A	B	C
5000	2390	1220	1480	1570	980	1420	1530	1210	2150
6000	2870	1470	1770	2170	1240	2070	1840	1460	2500
7000	3340	1710	2060	2360	1490	2310	2440	1700	3140
8000	3820	1950	2360	2560	1650	2550	2640	1950	3510

Table 3 Simulated electric field values (kV/m) around the tip of each nozzle of triangular array of nozzles at different applied voltages and having nozzle-to-nozzle gap of 5 mm

Applied Voltage (V)	Nozzle-1			Nozzle-2			Nozzle-3		
	A	B	C	A	B	C	A	B	C
5000	1320	1180	1380	1250	1180	1460	1270	1180	1390
6000	1580	1420	1650	1500	1410	1770	1520	1420	1690
7000	1850	1660	1930	1750	1650	1890	1770	1660	1880
8000	2110	1900	2210	2000	1880	2200	2030	1890	2290

Table 4 Simulated Electric field values (kV/m) around the tip of each nozzle of linear array of nozzles at different applied voltages and having nozzle-to-nozzle gap of 3 mm

Applied Voltage (V)	Nozzle-1			Nozzle-2			Nozzle-3		
	A	B	C	A	B	C	A	B	C
5000	1930	1210	1430	1370	960	1330	1270	1200	2020
6000	2250	1460	1720	1660	1120	1600	1520	1460	2420
7000	2780	1600	1900	1950	1390	1870	1780	1700	2820
8000	3010	1740	2020	2240	1530	2140	2030	1940	3220

Table 5 Simulated Electric field values (kV/m) around the tip of each nozzle of triangular array of nozzles at different applied voltages and having nozzle-to-nozzle gap of 3 mm

Applied Voltage (V)	Nozzle-1			Nozzle-2			Nozzle-3		
	A	B	C	A	B	C	A	B	C
5000	1380	1390	1185	1290	1380	1280	1320	1370	1220
6000	1520	1530	1480	1510	1580	1490	1560	1410	1340
7000	1760	1770	1670	1630	1760	1610	1690	1740	1610
8000	1900	1910	1670	1850	1890	1720	1880	2170	1790

3.2 End Effect

Due to the repulsive forces between the neighboring jets, the meniscus at the peripheral nozzles in an array of multi-nozzle emitter deflects outward as shown in Figure 6. This deflection is known as end-effect. It arises due to the asymmetric electric field around the meniscus of the end nozzles. Since end-effect has a direct relationship with the cross-talk between the neighboring jets i.e. end-effect increases with the increase in cross-talk between the neighboring jets. Therefore in this chapter it has been used as a measuring tool for the quantitative analysis of cross-talk between the neighboring jets.



Figure 6 Jetting image of triangular array multi-nozzle EHD inkjet printing head, showing deflection of the meniscus at the peripheral nozzles

3.3 Effects of Process Parameters on Cross-Talk

Cross-talk between the electrically charged neighboring jets is experimentally analyzed to determine its correlations with various process parameters, such as flow rate, applied voltage, nozzle-to-nozzle distance, nozzles array configuration, material composition of the printing nozzle, and nozzle diameter. In this section, the effects of these parameters on cross-talk are investigated through “end-effect”. The effect of each parameter is discussed in sections 3.3.1 to 3.3.6.

3.3.1 Flow Rate

The effect of flow rate on the cross-talk between the neighboring jets is investigated through jetting angle by changing the liquid flow rate while keeping the applied voltage constant. Figure 7 represents the variation of jetting angle with liquid flow rate at a constant applied voltage of 6 kV. Black and yellow lines represent nozzle 1 and nozzle 3 respectively. It is shown that with increase in flow rate, the jetting angle i.e. crosstalk between the neighboring jets decreases. Moreover the variation is more enhanced at low flow rate as compared to the high flow rate.

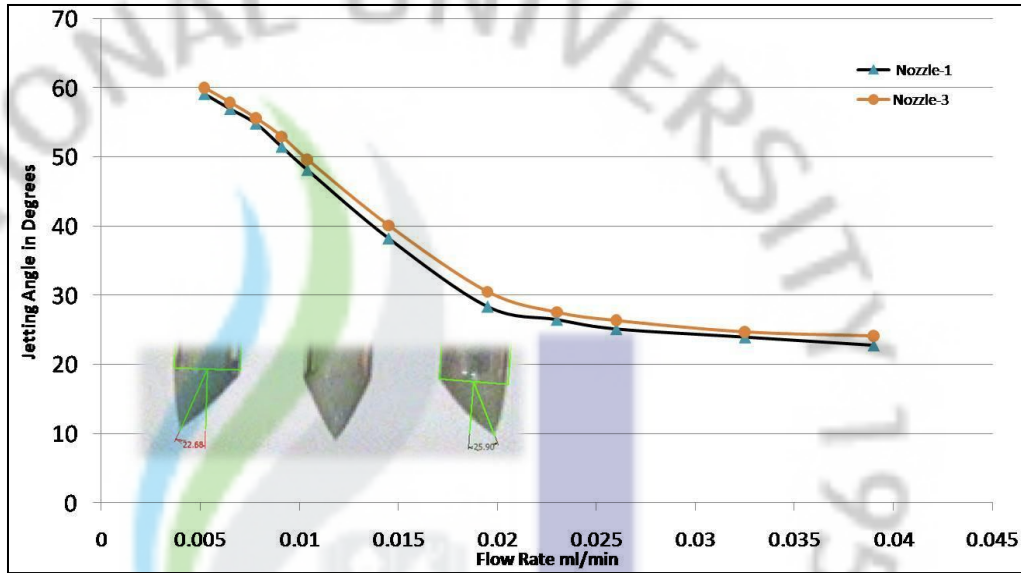


Figure 7 Jetting angles at boundary nozzles of a triangular array of nozzles, 3mm nozzle-to-nozzle gap and at constant applied voltage of 6kV

3.3.2 Applied Voltage

Influence of applied voltage on cross-talk i.e. jetting angle is investigated by keeping the flow rate constant. It is observed that the effect of applied voltage on jetting angle is opposite to that of the flow rate. Figure 8 illustrates the variation of the jetting angle with applied voltage at constant flow rate of 0.0026 ml/min for 3 mm nozzle-to-nozzle gap triangular array of nozzles. It is evident that jetting angle increases with the increase in applied voltage but unlike the influence of liquid flow rate the rate of change is almost constant.

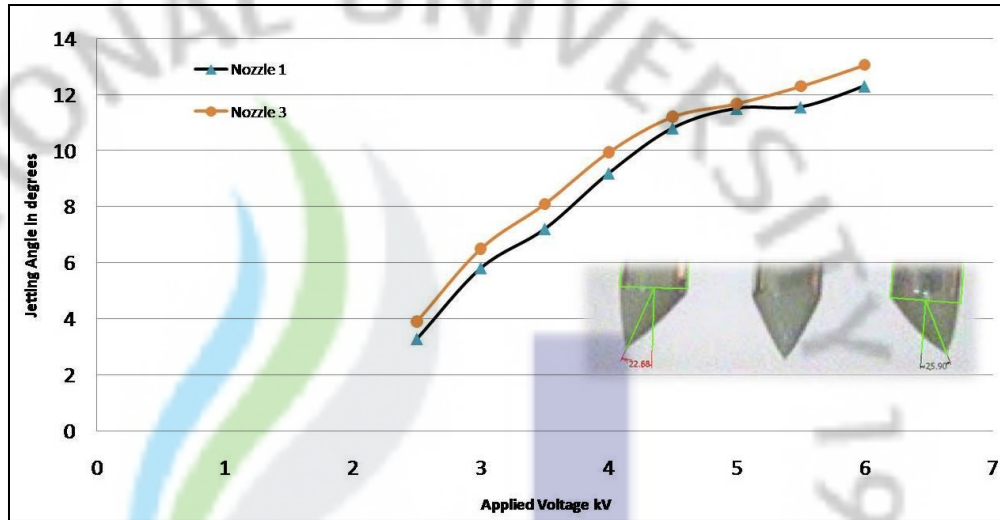


Figure 8 Jetting angles at boundary nozzles of a triangular array of nozzles, 3mm nozzle-to- nozzle gap and at constant flow rate of 0.0026 ml/min

3.3.3 Nozzle-to-Nozzle Distance

Jetting angle i.e. cross-talk between the neighboring jets increases with the decrease in space between the nozzles. Figure 9 shows the effect of applied voltage on the jetting angle at constant flow rate of 0.0026 ml/min for 5mm nozzle-to-nozzle gap triangular array of nozzles. It is evident from the comparison of both Figure 8 and Figure 9 that the influence of applied voltage is more enhanced in case of 3mm nozzle-to-nozzle gap as compared to 5 mm nozzle-to-nozzle distance. Also By comparing Table 3 and Table 5 it is clear that the electric field values are more asymmetric in case of 3mm nozzle-to-nozzle gap triangular array of nozzles. Therefore it can be concluded from the above comparisons that at small nozzle-to-nozzle distance, the neighboring jets experiences more cross-talk.

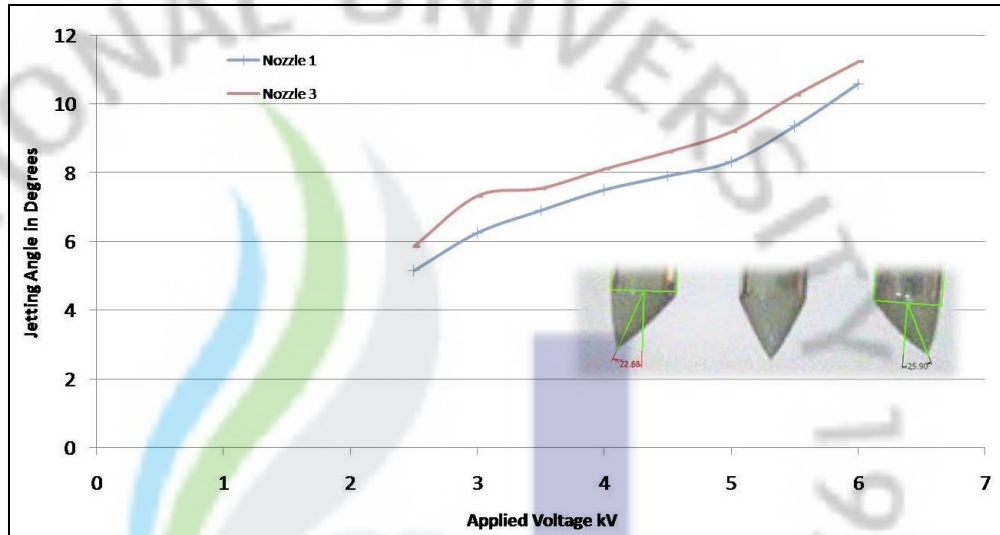


Figure 9 Jetting angles at boundary nozzles of a triangular array of nozzles, 5mm nozzle-to- nozzle gap and at constant flow rate of 0.0026 ml/min

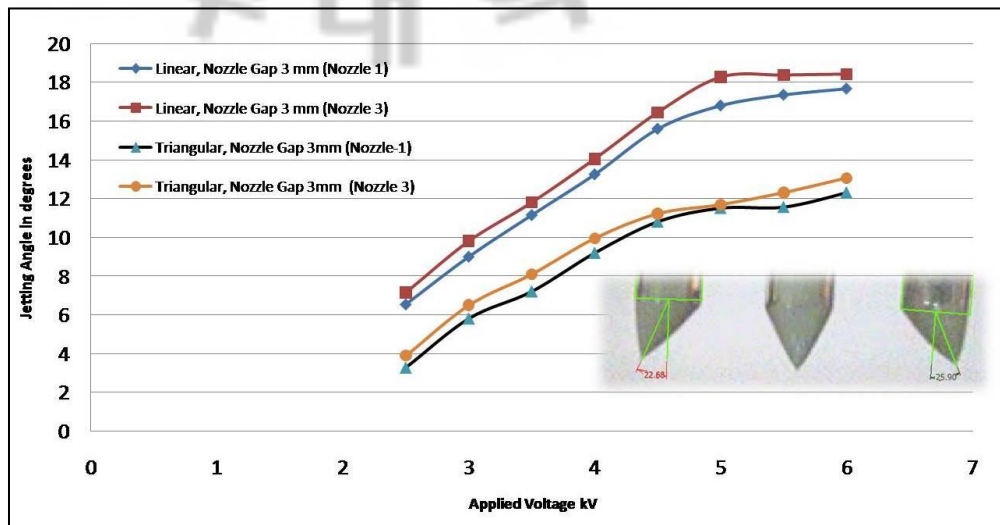
3.3.4 Nozzles Array Configuration

By comparing the electric field values of linear array of nozzles and triangular array of nozzles as given in Table 2 and Table 3 respectively, it is evident that in triangular array of nozzles the intensity of irregularity is low as compared to linear array of nozzles. Similarly in case of 3 mm nozzle-to-nozzle gap linear array of nozzles and the triangular array of nozzles as given in Table 4 and Table 5 respectively, the amount of indiscretion in triangular array of nozzles is less as compared to linear array of nozzles.

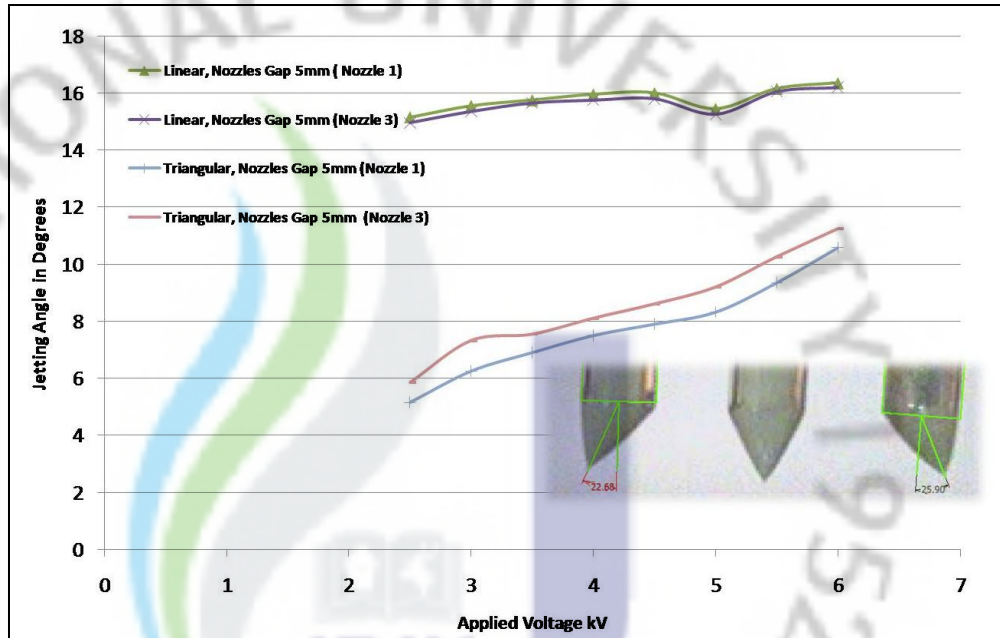
In order to cement the simulated results and experimentally investigate the effect of nozzles array configuration on cross-talk between the neighboring jets, experiments were performed on different array configurations (shown in Table 1). Jetting angles (amount of deflection of the meniscus from the center at the peripheral nozzles) were calculated on different voltages and fixed flow rate. Figure 10a presents the comparison of jetting angles between 3 mm nozzle-to-nozzle gap linear array of nozzles and 3 mm nozzle-to-nozzle gap triangular array of

nozzles. Similarly Figure 10b shows the comparison of jetting angles between 5 mm nozzle-to-nozzle gap linear array of nozzles and 5 mm nozzle-to-nozzle triangular array of nozzles. It is evident from both Figure 10a and Figure 10b that in triangular arrays, the values of jetting angle are about 30% and 60% small as compared to linear array of nozzles for the case of 3mm nozzle-to-nozzle gap and 5mm nozzle-to-nozzle gap respectively. This indicates that the triangular array of nozzles experiences less meniscus deflection at the end nozzles i.e. reduced end effect as compared to linear array of nozzles in EHD multi-nozzle inkjet printing process.

The reason for this trim down in meniscus deflection i.e. “end effect” is that while using the triangular array of nozzles instead of linear array of nozzles, the apparent nozzle-to-nozzle distance increases while the actual distance between the printing lines remains constant. As a result of this increase in nozzle-to-nozzle gap, 30% to 60% less deflection has been observed at the end nozzles of triangular arrays of nozzles for different nozzle gap arrangements.



(a)



(b)

Figure 10 Comparison of jetting angles at boundary nozzles of linear array multi-nozzle EHD inkjet printing head and triangular array multi-nozzle EHD inkjet printing head (a) 3mm nozzle-to-nozzle gap, at different applied voltages and constant flow rate of 0.026 ml/min (b) 5mm nozzle-to-nozzle gap, at different applied voltages and constant flow rate of 0.0013 ml/min

3.3.5 Material Composition of the Printing Nozzle

Material composition of the printing nozzles has dominant effect on the cross-talk between the neighboring jets. Generally, the use of metallic nozzles strengthens the repulsive force between the neighboring jets as compared to nozzles made of a dielectric material. Therefore, to minimize the cross-talk between the neighboring jets, multi-nozzle inkjet printing heads used in the experiments were completely fabricated from dielectric (glass and PDMS) or insulator (ABS) materials.

3.3.6 Nozzle Diameter

In multi-nozzle EHD inkjet printing process, the use of smaller printing nozzles offers a favorable advantage on the cross-talk between the neighboring jets i.e. with the decrease of nozzle size, cross-talk between the neighboring jets decreases [31]. In other words, by using small size printing nozzles the distance between adjacent nozzles can be significantly decreased. However on the other hand side, a well known problem of inkjet printers i.e. nozzle blockage is also associated with the usage of small sized nozzles. Therefore optimization of the nozzle size is required for deposition of any colloidal solution though multi-nozzle EHD inkjet printing process.

4. Experimental Methods

Presently, EHD printing platforms are only in laboratories. Several platform and prototype have been built and tested for printing of a variety of materials. The main challenge is related with the facts that only at particular flow rates and high-voltage electric field, a cone-jet configuration with uniform jet/droplet size can be obtained. In the present work, a customized multi-nozzle EHD inkjet printing rig has been developed. For the first time, a multi-channel pump and a voltage distributor are used for individual ink supply and voltage supply to each nozzle respectively.

In this chapter, the details of multi-nozzle EHD inkjet printing head development, experimental setup and instrumentation are presented. Section 4.1 describes the type and properties of inks used for experiments. Section 4.2 focuses on the multi-nozzle EHD inkjet printing head fabrication and is divided into three subsections. Section 4.2.1, Section 4.2.2 and Section 4.2.3 outlines the fabrication methodology of 3ND multi-nozzle EHD inkjet printing head, 5ND multi-nozzle EHD inkjet printing head and 5NI multi-nozzle EHD inkjet printing head respectively. Finally, the experimental set-up used for multi-nozzle EHD inkjet printing process is presented in Section 4.3.

4.1 Inks Used

For printing metallic patterns, two types of conductive inks (the inks based on the metal nanoparticle suspension known as colloidal solution and the organo-metallic compounds) are commonly used in printed electronics. In this work both types of inks i.e. colloidal solutions

(containing silver nanoparticles and copper nanoparticles) and organo-metallic compound (organo-silver) are printed. The details of each ink are given in the following subsections.

4.1.1 Silver Colloidal Solution

Silver is one of the most important materials in electronic microstructures because of its high conductivity, chemical stability and resistance to surface oxidation [32]. A number of research groups have focused on direct printing of a colloidal solution containing silver nanoparticles for fabrication of electrically functional microstructures [33, 34] and micro-tracks [35–37] using a single-nozzle EHD inkjet printing head. In this dissertation, a commercial silver colloidal ink (npk-020, NPK.CO) was used for fabrication of electrically functional microstructures. The properties silver colloidal ink is provided by the supplier and is given in Table 6.

Table 6 Properties of silver colloidal solution used for experiments

Property	Value
Resistivity (Ω -cm)	1.051E+5
Viscosity (Pa*s)	0.039
Surface Tension (N/m)	0.005
Nanoparticles Weight (%)	39
Average particle size (nm)	30

4.1.2 Copper Colloidal Solution

In EHD printing process, most of the relevant studies have focused on direct printing of colloidal solutions containing novel metals such as silver and gold nanoparticles for their high conductivity and non-oxidizing properties. However, these metals are too expensive to be used for mass production of electronic devices, thus we need to seek an alternative that is inexpensive, highly conductive, and air stable. Because of its lower cost and less electro-migration effect than other metals, recently colloidal solutions containing copper nanoparticles were shown as a promising alternative for silver or gold-based inks in fabrication of microelectronic structures. Hong and Wagner successfully fabricated source and drain electrodes of thin-film transistor using copper nano-ink through piezoelectric inkjet printer [38]. Park et al. patterned copper nanoparticles onto glass substrates through piezoelectric inkjet printing process, exhibiting an electrical resistivity of $17.2 \mu\Omega\cdot\text{cm}$ [39]. Lee et al. printed copper nano ink onto polyimide substrates using piezoelectric inkjet printing technique resulting in metallic copper traces having an electrical resistivity of $3.6 \mu\Omega\cdot\text{cm}$ [40]. Kang et al. used piezoelectric inkjet printer for direct deposition of copper nanoparticles for PCB's electrodes fabrication showing an electrical resistivity of $3.67 \mu\Omega\cdot\text{cm}$ [41]. Yung and Plura processed copper nanoparticle onto polyimide substrate using piezoelectric inkjet printer and turned them into soldered structures using an Nd-YAG laser [42]. Due to the above potential applications in printed electronics, recently we pioneered the EHD inkjet printing process of copper colloidal solution using single nozzle printing head [43]. In this dissertation, copper colloidal ink used was obtained from Korea Research Institute of Chemical Technology (KRICT) and was successfully printed using multi-nozzle EHD inkjet printing process. The properties silver colloidal ink is provided by the supplier and is given in Table 7.

Table 7 Properties of copper colloidal solution used for experiments

Property	Value
Conductivity (S/m)	7.50E-3
Viscosity (Pa*s)	7.60E-3
Surface Tension (N/m)	3.69E-2
Electric Permittivity (ϵ)	48.5
Nanoparticles weight (%)	40
Average Particle Size (nm)	20

4.1.3 Organo-Metallic Ink

Organo-metallic ink has received special interest in direct printing for its true-solution property, where the metal salt is fully dissolved in the solvent. This property is desirable for the EHD inkjet printing technology as it can effectively reduce the sediment and clogging issues arising from nanoparticles in the suspension. Additionally, a low process temperature for thermal decomposition is required with the organo-metallic compounds, instead of the high temperature associated with sintering nanoparticles. These features make the organic inks quite favorable for printing. For printing in this dissertation, a commercially available silver organo-metallic ink (TEC-IJ-020) was obtained from InkTec Elec., South Korea. The physical properties of the ink are listed as in Table 8.

Table 8 Properties of silver organo-metallic ink used for experiments

Property	Value
Viscosity (Pa*s)	1.5E-3
Surface Tension (N/m)	3.2E-2
Silver weight (%)	20

4.2 Development of Multi-Nozzle EHD Inkjet Printing Head

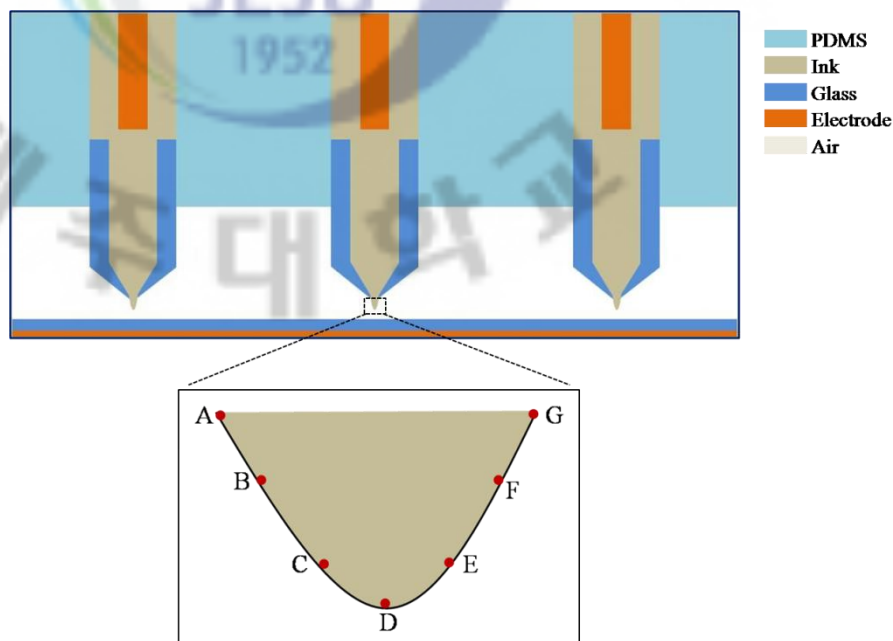
In the present work, three types of multi-nozzle EHD inkjet printing heads were used for printing of colloidal solutions. First, a prototype multi-nozzle EHD inkjet printing head consisting of three nozzles and having discrete counter electrode were fabricated and successfully tested for deposition of silver colloidal solution. Then, this prototype head has been improved to a multi-nozzle EHD inkjet printing head consisting of five nozzles and having discrete counter electrode were developed and successfully tested for printing of copper colloidal solution. Finally, the prototype multi-nozzle head been improved to a multi-nozzle EHD inkjet printing head consisting of five nozzles and having integrated counter electrode. In this dissertation for simplicity, from now on the term “3ND multi-nozzle EHD inkjet printing head” has been used for multi-nozzle EHD inkjet printing head consisting of three nozzles and having discrete counter electrode. Similarly, the name “5ND multi-nozzle EHD inkjet printing head” has been used for multi-nozzle EHD inkjet printing head consisting of five nozzles and having discrete counter electrode and “5NI multi-nozzle EHD inkjet printing head” has been used for multi-nozzle EHD inkjet printing head consisting of five nozzles and having integrated counter electrode. The simplified steps involved in the development and fabrication of each head is presented in the following subsections.

4.2.1 3ND Multi-Nozzle EHD Inkjet Printing Head

In EHD inkjet printing, the jet emanates from that point of liquid meniscus where the electric charge density i.e. the electric field strength has the highest magnitude [7]. In case of single nozzle EHD inkjet printing the jet emanates from the center point of the meniscus, since it is the point of maximum electric field strength. However, in case of multi-nozzle EHD inkjet

printing, due to the cross-talk i.e. repulsive force between the neighboring jets the point of highest electric field strength becomes slightly off center especially at peripheral nozzles, resulting in emission of outward-tilted jets [44]. As discussed in Section 3-3 that the two factors that have dominant effect on the cross-talk between the neighboring jets are the distance between the adjacent nozzles of the EHD inkjet printing head and the material composition of the printing nozzles. Therefore, to minimize the cross-talk between the neighboring jets, multi-nozzle inkjet printing heads were completely fabricated from dielectric materials i.e. glass and PDMS. Moreover, to find the minimum distance at which the adjacent jets experience no cross-talk, numerically simulated values of electric field strength at various points of the meniscus of each nozzle has been investigated by commercially available finite element software COMSOL (3.5a, Comsol Inc.). Figure 11a shows the schematic of the FEA model used for electric field simulation of multi-nozzle EHD inkjet printing head. Six FEA models were developed having the same configuration (Figure 11a) but with different nozzle-to-nozzle distances i.e. 500 μ m, 1mm, 1.5mm, 2mm, 2.5mm and 3mm. Simulations were run by applying a dc voltage of 3.5 kV at the boundaries of each electrode. The parameters used for simulation are summarized in Table 8. Numerical values of electric field strength at seven different points i.e. A, B, C, D, E, F, G (as shown in Figure 11a) around the meniscus of each nozzle have been calculated for each model. It is observed from electric field simulation results that all models having nozzle-to-nozzle distance less than 3mm, the point of maximum electric field strength is not at the center of the meniscus for peripheral nozzles. For comparison, the resulting values of electric field strength around the tip of each nozzle of 2.5 mm nozzle-to-nozzle distance and 3mm nozzle-to-nozzle distance are enlisted in Table 9 and Table 10 respectively. The data in Table 9 shows that at the meniscus of nozzle 1, the electric field strength has maximum value at point 'C' while at the meniscus of

nozzle 3; the electric field strength has maximum value at point 'E'. Since both point 'C' and point 'E' are not the central points of the meniscus therefore, the emanated jets will be off center and will fall away from the targeted position on the substrate. On the other hand, it is evident from the data in Table 10 that in case of 3mm nozzle-to-nozzle distance the electric field strength has maximum value at point 'D' (center point) of each nozzle, which means that the jets will emanate from center of the meniscus of each nozzle. The resulted electric field values for the case of 3mm nozzle-to-nozzle distance are also shown in Figure 11b. Following the simulated results, multi-nozzle printing head consists of three nozzles and having 3mm nozzle-to-nozzle distance has been fabricated.



(a)

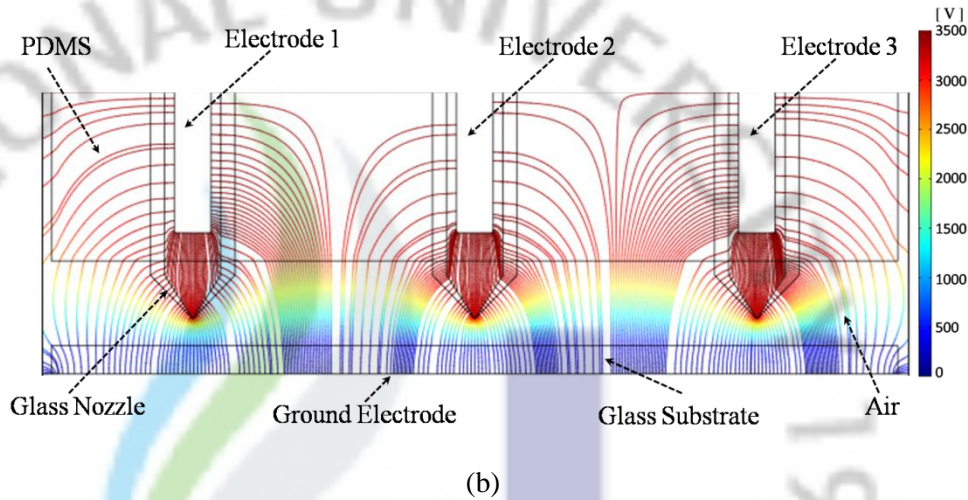


Figure 11 (a) of the FEA model used for electric field simulation (b) Simulation in COMSOL 3.5a of the electric field lines

Table 9 Details of electric field simulation parameters used for analysis.

Parameter	Type/Value
Model	2D Electrostatic
Solver	UMFPACK
Mesh	Triangular
Number of Mesh Elements	57184
No. of Boundary Elements	2508
Average Element Area Ratio	2.9E-5
Relative Tolerance	1.0E-6

Table 10 Simulated Electric field (kV/m) values around the meniscus of each nozzle on different points at an applied voltage of 3.5 kV and nozzle-to-nozzle gap of 2.5 mm.

Nozzle/ Point	A	B	C	D	E	F	G
Nozzle 1	315	530	740	610	570	325	240
Nozzle 2	230	295	510	700	510	290	230
Nozzle 3	235	320	550	600	735	520	310

Table 11 Simulated Electric field (kV/m) values around the meniscus of each nozzle on different points at an applied voltage of 3.5 kV and nozzle-to-nozzle gap of 3 mm.

Nozzle/ Point	A	B	C	D	E	F	G
Nozzle 1	260	320	550	730	545	310	245
Nozzle 2	240	300	520	710	520	295	240
Nozzle 3	250	315	540	735	550	320	260

3ND Multi-nozzle EHD inkjet printing head having discrete i.e. plate as a counter electrode is consisted of three parts i.e. Poly Di-Methyl Siloxane (PDMS) holder, glass nozzles and copper electrodes. Procedure followed for the individual part fabrication and assembling of these parts into a complete multi-nozzle EHD inkjet printing head is given below.

First, PDMS holder was fabricated in-house by using the standard soft lithography technique. The selection of PDMS for capillaries' holder is primarily motivated by its low cost, dielectric disposition, hydrophobic nature, desirable optical properties and low thermal expansion constant. Figure 12a shows the simplified fabrication steps involved in mold preparation. Three 4mm and three 3mm long stainless steel circular rods each having 1.5mm

outer diameter were partially inserted through small drilled holes into two rectangular Poly Methyl Meth-Acrylate (PMMA) plates of size 15.5mm × 6.5mm and 14.5mm × 5.5mm respectively. The plates (with inserted rods) were then assembled to form an open shaped mold. PDMS mixture consisted of a Sylgard 184 silicone elastomer base and curing agent (Dow Corning, Midland) that were mixed in a ratio of ten parts base to one part curing agent by mass. The prepolymer mixture was poured onto the mold and degassed at 5–10 Pa in a desiccator with a mechanical vacuum pump (KH201, Koino) for 1h to remove any air bubbles in the mixture and to insure complete mixing of the two parts. The PDMS prepolymer was then cured for 1h at 100 °C on a hot plate. After curing, the PDMS replicas were peeled off from the mold leaving three L-shaped (having three 1.5mm inlet and three 1.5mm outlet channels) flow-ready channels. Since the stainless steel rods used to mold the channels were very smooth therefore the process of removing them from the cured PDMS did not introduce imperfections from tearing or rubbing. The schematic of final PDMS holder is shown in Figure 12.

Then, three Glass capillary tubes of 1.5 mm outer diameter and 0.75 mm inner diameter (BF 150, Sutter Instrument) were pulled and micro-nozzles were formed, each with sharp tip of 100µm inner diameter and ≈140–170µm outer diameter by using a micropipette puller (P-97, Sutter Instrument). These glass capillaries were then inserted in the outlet channels of the PDMS holder. Finally, three copper electrodes having outer diameter of 500 µm were inserted from the top of the PDMS holder. The complete schematic of 3ND multi-nozzle EHD inkjet printing head is shown in Figure 12c. Also the photograph of the 3ND multi-nozzle EHD inkjet printing head is shown in Figure 13.

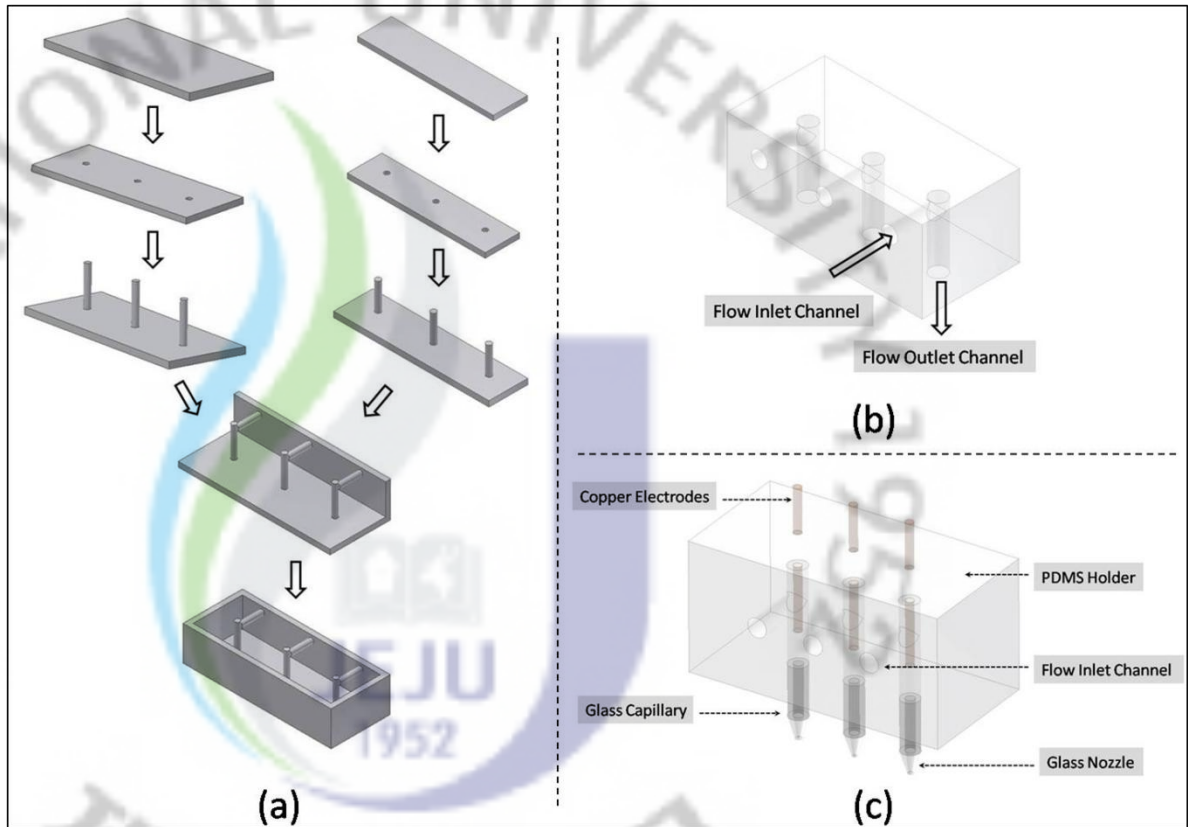


Figure 12 Schematic illustration of the 3ND multi-nozzle EHD inkjet printing head fabrication process: (a) Simplified fabrication steps of mold preparation (detailed drawing is shown in appendix A) (b) Resulted PDMS holder having L-shaped channels for ink supply and clamping of glass capillaries (c) Complete multi-nozzle EHD inkjet printing head

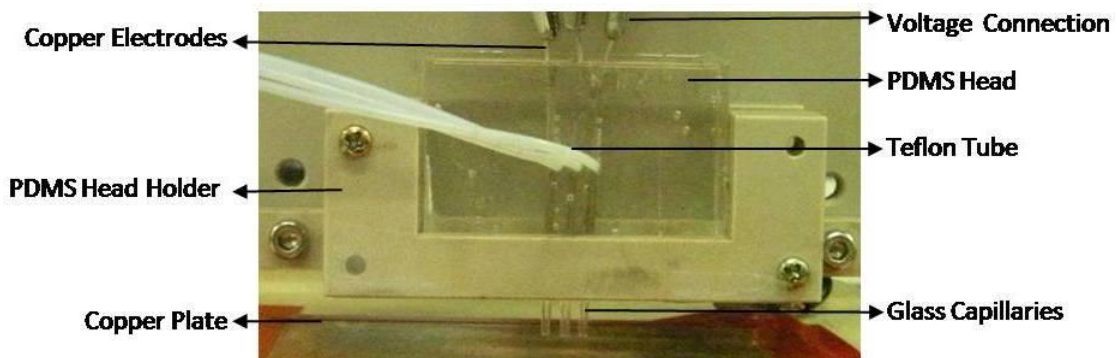


Figure 13 Photograph of the 3ND multi-nozzle EHD inkjet printing head

4.2.2 5ND Multi-Nozzle EHD Inkjet Printing Head

In multi-nozzle EHD inkjet printing process, the use of smaller printing nozzles offers a favorable advantage on the cross-talk between the neighboring jets i.e. with the decrease of nozzle size, cross-talk between the neighboring jets decreases [31]. In other words, by using small size printing nozzles the distance between adjacent nozzles can be significantly decreased. However on the other hand side, a well known problem of inkjet printers i.e. nozzle blockage is also associated with the usage of small sized nozzles. Therefore optimization of the nozzle size is required for deposition of any colloidal solution through EHD inkjet printing process. In this study, the optimal nozzle size (minimum nozzle size at which the nozzle is not blocking) was selected for copper colloidal solution. Procedure followed for the optimization of all these parameters is given below.

In order to find the optimal nozzle size for the printing of a particular colloidal solution, first experiments were performed on printing of that particular colloidal solution using a single nozzle EHD inkjet printing head. Different nozzles, having internal diameter of 10 μm , 15 μm , 20 μm , 25 μm , 30 μm were tested for blockage respectively by supplying copper colloidal solution for some time. It was observed that all nozzles were get blocked by the copper nano-ink except the nozzle having internal diameter of 30 μm . Therefore, the nozzle having internal diameter of 30 μm was chosen for deposition of copper colloidal solution.

After successful testing of 3ND multi-nozzle EHD inkjet printing head, same procedure was followed for the fabrication of 5ND multi-nozzle EHD inkjet printing head. The simplified steps involved in 5ND multi-nozzle EHD inkjet printing head fabrication are shown in Figure 14. Finally, while using nozzles having 30 μm sizes and by following the same nozzle to nozzle distance optimization methodology of 3ND multi-nozzle EHD inkjet printing head, 2mm nozzle-

to-nozzle distance was observed to be the minimum distance at which the adjacent jets experience no cross-talk.

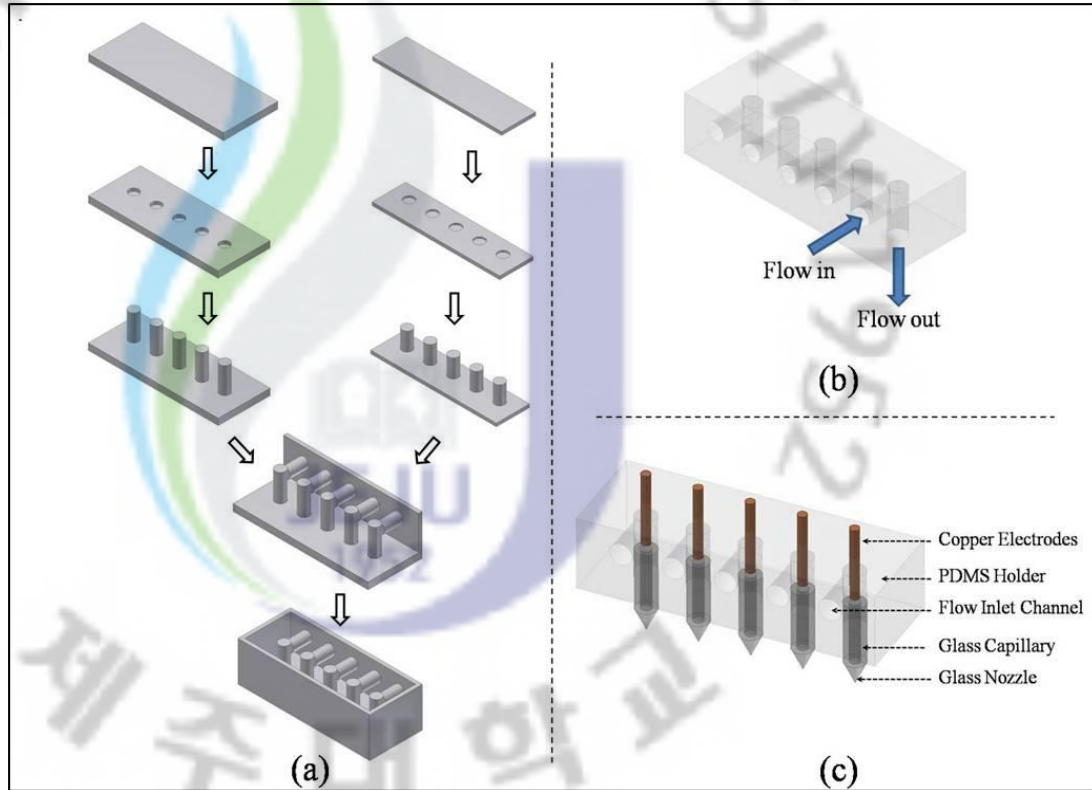


Figure 14 Schematic illustration of the multi-nozzle EHD inkjet printing head fabrication process: (a) Simplified fabrication steps of mold preparation (detailed drawing is shown in appendix B) (b) PDMS holder having L-shaped channels for ink supply (c) Complete multi-nozzle EHD inkjet printing head

4.2.3 5NI Multi-Nozzle EHD Inkjet Printing Head

In both the above multi-nozzle EHD inkjet printing heads, discrete counter/ground electrodes have been used where the substrate is in between the terminals. As a result of which the printing parameters are also affected by the properties of the substrate used. To avoid the effects of substrate on the printing parameters, a multi-nozzle inkjet printing head (5NI) design consisting of five nozzles and having integrated counter electrode has been proposed. In this multi-nozzle inkjet print head, substrate effects on printing parameters are eliminated by placing

the ring shaped ground electrodes above the substrate. The schematic and photograph of the 5NI multi-nozzle EHD inkjet printing head are shown in Figure 15 and Figure 16 respectively. Also the detailed drawings of the individual parts of the holder are presented in Appendix C.

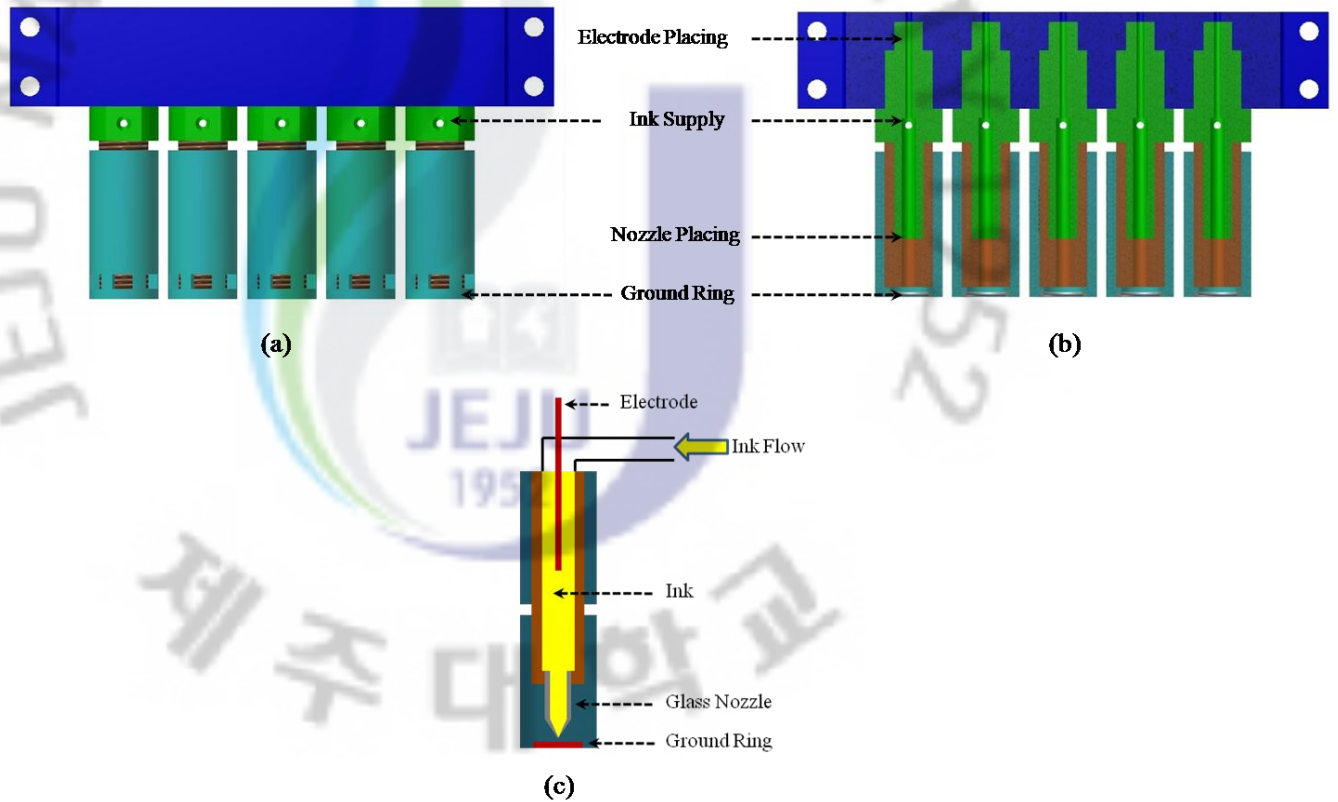


Figure 15 Schematic illustrations of 5NI multi-nozzle EHD inkjet printing head (a) Holder for the nozzle and the ground ring (b) cross-sectional view of the holder (c) complete printing head

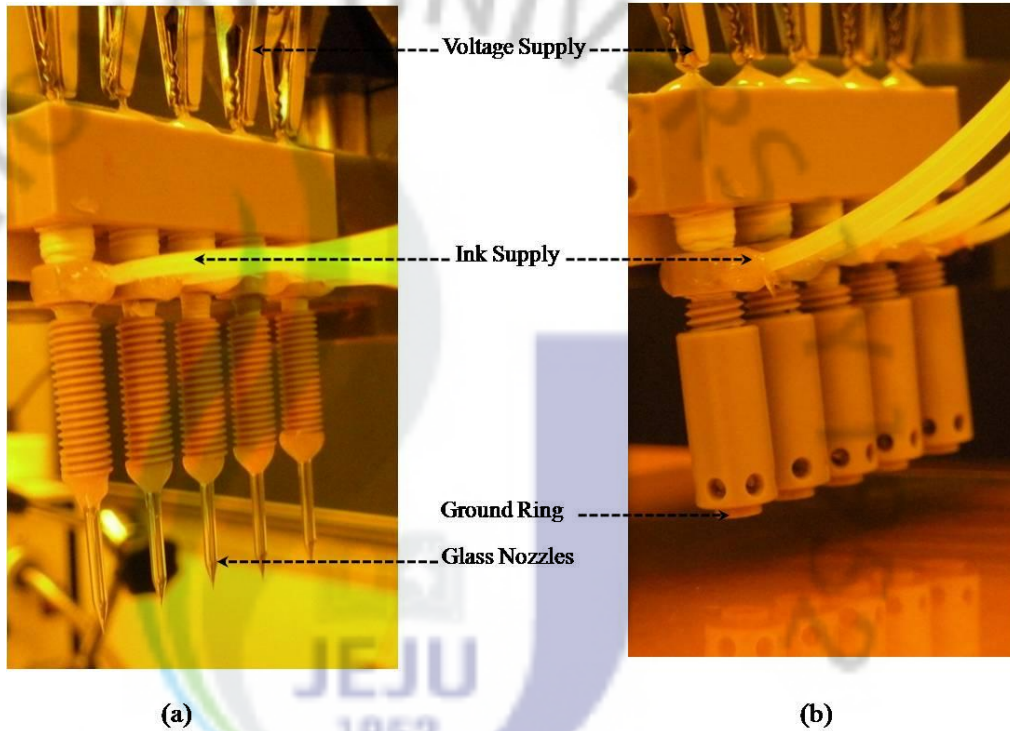
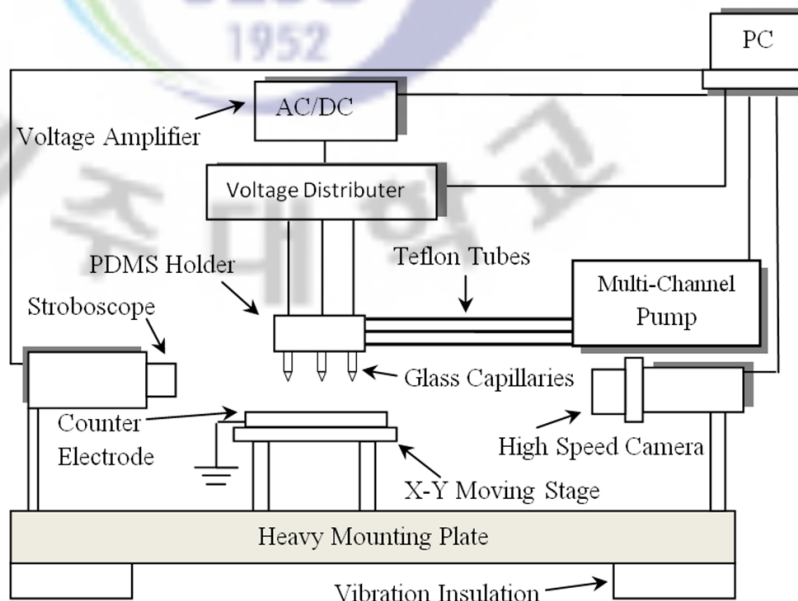


Figure 16 Photograph of 5NI multi-nozzle EHD inkjet printing head (a) without integrated ground ring (b) with integrated ground ring

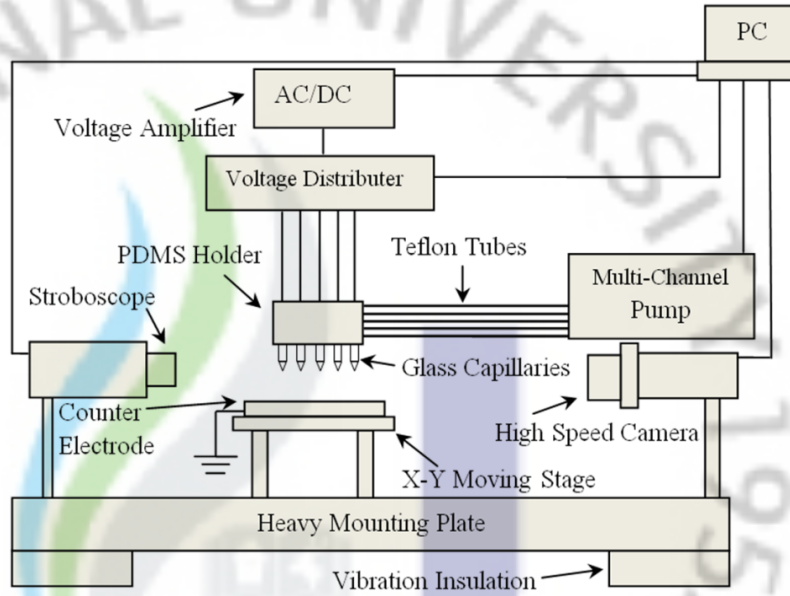
4.3 Experimental Set-Up

For all experiments lab developed set-up was used. Figure 17a, 17b and 17c show schematic diagrams of 3ND multi-nozzle EHD inkjet printing head, 5ND multi-nozzle EHD inkjet printing head and 5NI multi-nozzle EHD inkjet printing head respectively. The multi-nozzle EHD printing head was held in a holder made of acrylic. In order to supply voltage to each nozzle, all the nozzles were connected to a voltage distributor (HM10-5, Hanmac) through copper electrodes which were further connected to a high-voltage power supply (10/40 A, Trek). The inlet channels of the PDMS holder were connected to a multi-channel pump (IP-RS232, Ismatec) through Teflon tubes for individual ink supply to each nozzle. A copper plate was placed on an X–Y moving stage below the nozzle exits as ground/counter electrode for both

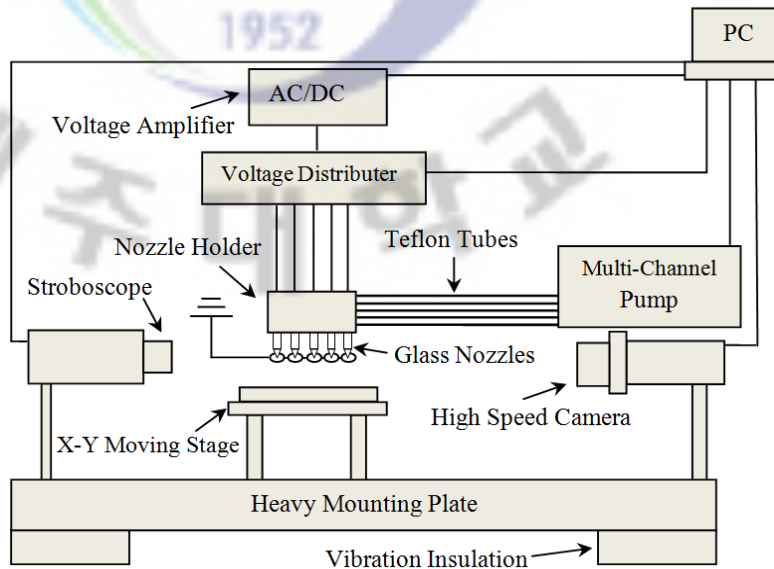
3ND multi-nozzle EHD inkjet printing head and 5ND multi-nozzle EHD inkjet printing head. Glass substrates having 500- μm thickness were placed on top of the ground plate. The behavior of the jetting was monitored with the help of a high-speed camera (X3, 11X, 5000 fps, Motion Pro). A high-voltage power supply, multi-channel pump, high-speed camera, moving stage (for substrate motion) and the head holder (for adjustment of the distance between nozzles and ground plate) were connected through a hardware system (PXI-1042Q, National Instruments), controlled by laboratory-developed software based on LabVIEW. Moreover, the amplitude and waveform of the applied voltage were also controlled with the help of this customized software. The photograph of the laboratory-developed E-jet printing rig is shown in Figure 18.



(a)



(b)



(c)

Figure 17 Schematic illustrations of experimental setups using (a) 3ND multi-nozzle EHD inkjet printing head (b) 5ND multi-nozzle EHD inkjet printing head (c) 5NI multi-nozzle EHD inkjet printing head

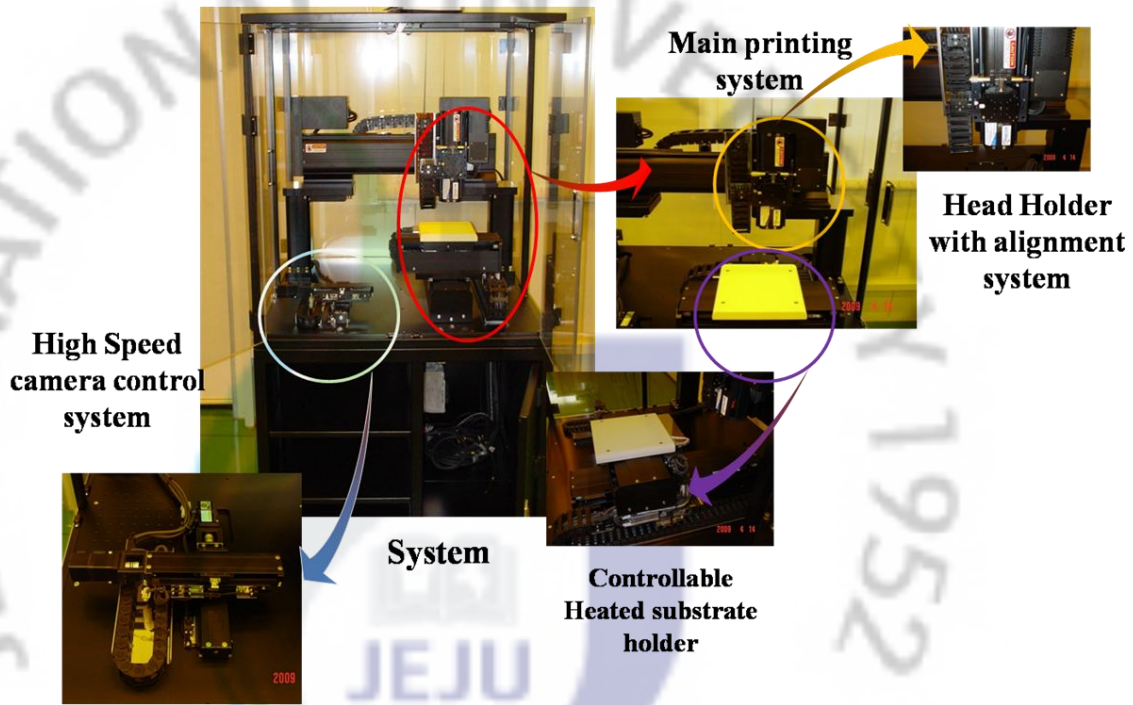


Figure 18 Photograph of EHD inkjet printing rig used for experiments

5. Printed Results and Characterization

In this chapter, printed results of the multi-nozzle electrohydrodynamic (EHD) inkjet printing heads are reported. Multi-nozzle EHD inkjet printing heads (Section 4.2) were successfully tested by simultaneously printing electrically conductive tracks of colloidal solutions (Section 4.1) onto the glass substrate. The printed tracks are analyzed both physically and electrically by using different characterization tools such as optical microscopy, scanning electron microscopy (SEM), atomic force microscopy (AFM), X-ray diffraction (XRD) and four point probe. Section 5-1, Section 5-2 and Section 5-3 present the printed results of 3ND multi-nozzle EHD inkjet printing head, 5ND multi-nozzle EHD inkjet printing head and 5NI multi-nozzle EHD inkjet printing head respectively.

5.1 Results of 3ND Multi-Nozzle EHD Inkjet Printing Head

In this section, the printed results of the Multi-nozzle EHD inkjet printing head consisting of three nozzles and having discrete counter electrode (plate) are presented. 3ND multi-nozzle EHD inkjet printing head was successfully tested by simultaneously printing electrically conductive lines of colloidal solution containing silver nanoparticles onto the glass substrate. The details and characterization of the printed results are illustrated in the following subsections.

5.1.1 Axisymmetric Micro-jet Generation

Due to dielectric properties of glass and optimized nozzle-to-nozzle distance i.e. 3 mm (section 4.1.1), cross-talk between the adjacent jets had not been observed. Figure 19 shows high

speed camera images of a stable meniscus formed at the tip of individual nozzles of the multi-nozzle EHD inkjet printing head. Axisymmetric Taylor cones were formed at the tip of each nozzle, i.e. nozzle 1, nozzle 2 and nozzle 3, whose pinnacle emitted very small jets ($10 \pm 2 \mu\text{m}$) at an applied dc voltage and flow rate of 3.5 kV and $20 \mu\text{l/h}$, respectively.



Figure 19 Photographs of axisymmetric liquid menisci established at the nozzle tips of 3ND multi-nozzle EHD inkjet printing head

5.1.2 Printed Results on Glass Substrate

Controlling the morphology of the printed conductive pattern plays an important role to determine its electrical conductivity and mechanical adhesion property. Furthermore, the conductive patterns with a non-uniform surface are generally unsuitable for use in multilayer interconnect structures, since overlying different components are prone to pin holes due to the poor coverage of the numerous ridges and valleys [45]. Experimental parameters such as ink flow rate, applied voltage and traveling time of the jet, i.e. nozzle to substrate distance, have a great effect on the morphology of printed patterns. Therefore, these parameters need to be optimized in order to get printed lines of uniform microstructure [46]. Optimizing the experimental parameters, printing was performed by applying a dc voltage of 3.5 kV and a flow rate of $20 \mu\text{l/h}$ to each nozzle. The nozzle to substrate distance was set at $300 \mu\text{m}$ while the substrate speed was kept constant at 10 mm/s . Figure 20 shows the high zoom static camera and

optical microscope image of continuous silver tracks simultaneously printed by three nozzles on a glass substrate without any defects such as bulges or coffee-ring effects [47]. Since the substrate, i.e. glass, has a hydrophilic surface, the deposited jets were able to spread out so that the width of the lines became larger than the original sizes of the generated jets ($10 \pm 2 \mu\text{m}$). The average line width of the printed lines is $140 \mu\text{m}$ with a standard deviation of $5 \mu\text{m}$.

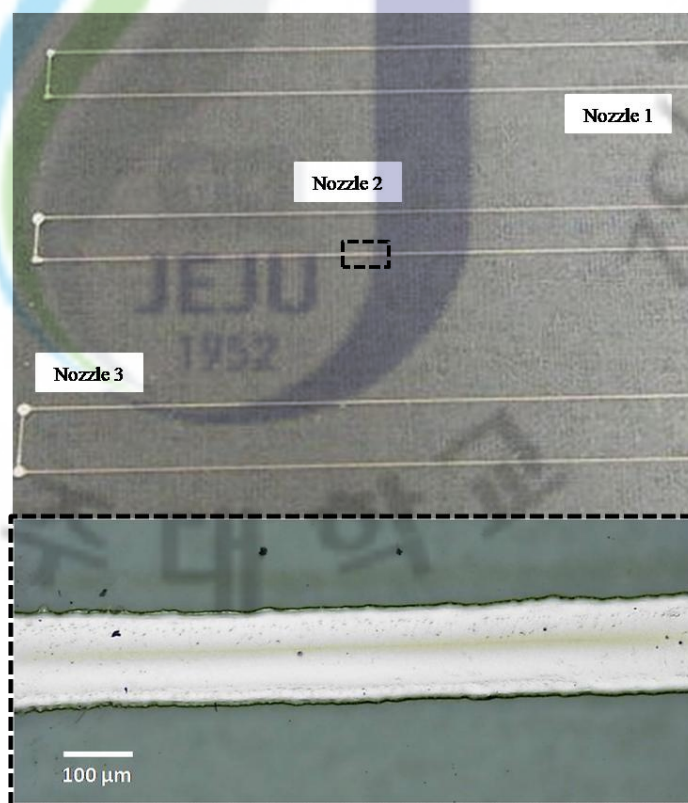


Figure 20 High-zoom static camera and optical microscope image of continuous silver lines printed on glass substrate by 3ND multi-nozzle EHD inkjet printing technique. The bottom inset shows the average line width of $140\mu\text{m}$.

5.1.3 X-ray diffraction Analysis of the Printed Lines

Figure 21 shows the X-ray diffraction (XRD) spectrum of a typical continuous track printed by the multi-nozzle EHD inkjet printing process. The diffraction peaks correspond to the (111), (200), (220) and (311) planes, respectively. Since the phases in Figure 21 show the

existence of silver only, it is confirmed that the material of the printed line consisted of silver nanoparticles only.

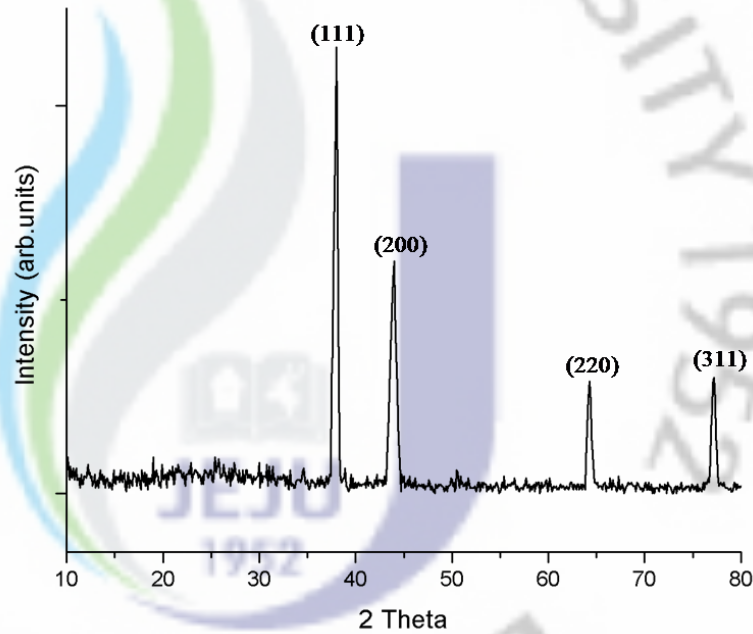


Figure 21 X-ray diffraction (XRD) spectrum of the printed line

5.1.4 Scanning Electron Microscopy of the Printed Lines

The scanning electron microscopy (SEM) images of a typical line printed by 3ND multi-nozzle EHD inkjet printing head (Figure 22) illustrate that the nanoparticles are three-dimensionally interconnected with each other, which favorably affects the electrical conductivity.

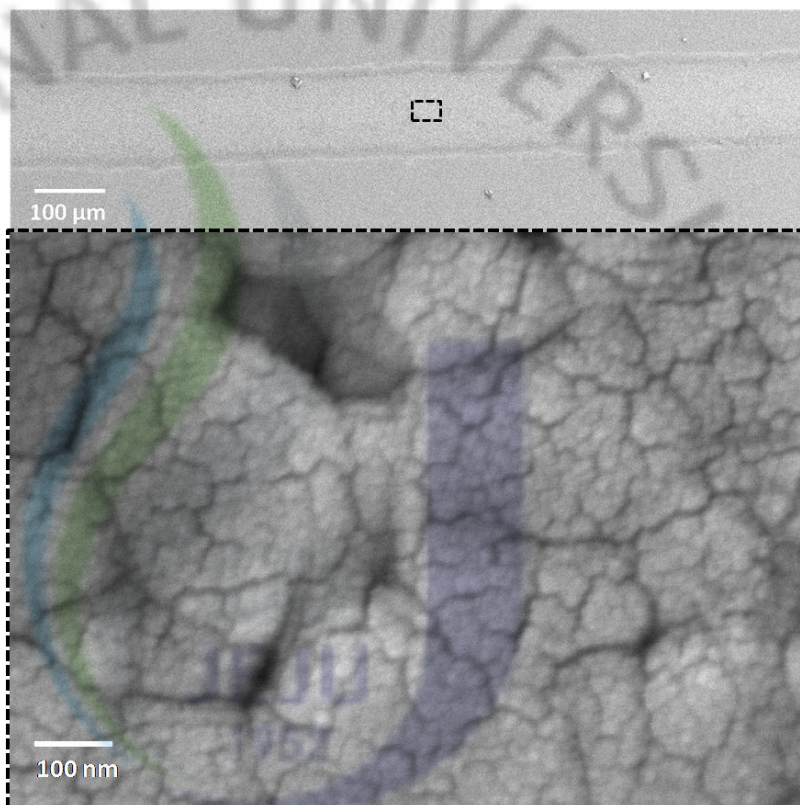
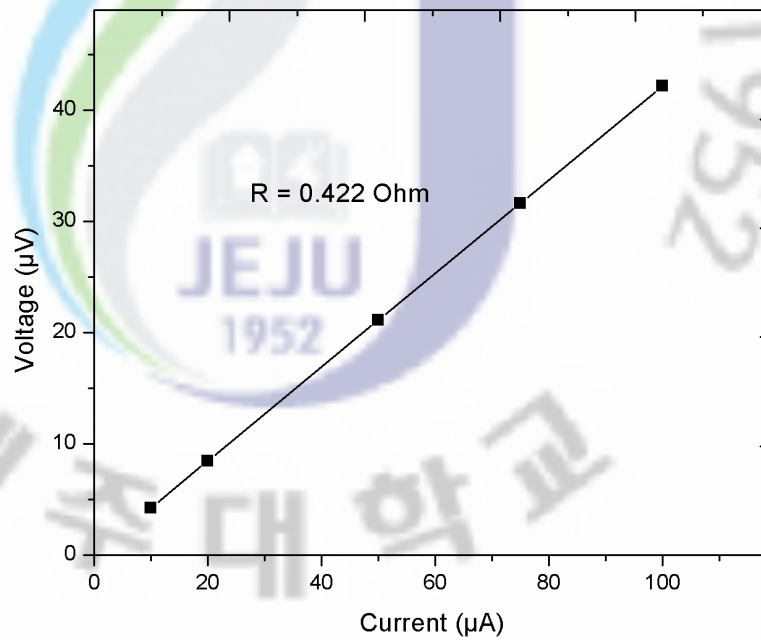


Figure 22 SEM image of continuous silver track deposited by 3ND multi-nozzle EHD inkjet printing head. The bottom inset shows the three-dimensionally interconnected silver nanoparticles

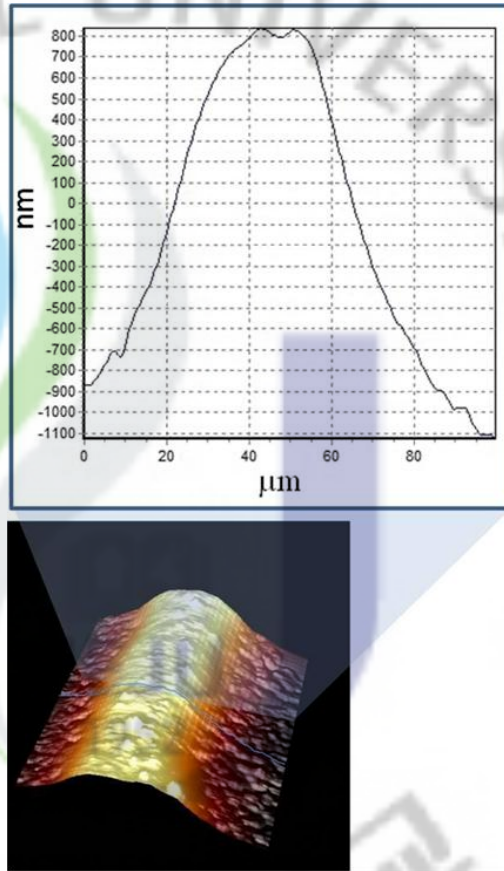
5.1.5 Electrical Characterization of the Printed Lines

After sintering at 250°C, for 1h at a constant heating rate of 2°C/min, the resistance R of the printed silver lines was measured by using standard 4-point method. Linear Ohmic I-V curve (Figure 23a) was obtained by measuring voltage drop ΔV across a 1.5 mm long sample of printed line by applying current I of different intensity (10μA, 20μA, 50μA, 75μA, 100μA). The electrical resistivity ρ of printed lines was then calculated from the resistance R , the length L , and the cross sectional area A of the line using $\rho = R \cdot A / L$. Cross-sectional area was determined by numerical integration of measured profile from the atomic force microscopy (AFM) image of the printed line shown in Figure 23b. The value of resistivity was calculated to be $5.05 \times 10^{-8} \Omega \cdot \text{m}$

which is almost three times high as compared to bulk silver resistivity at room temperature ($1.59 \times 10^{-8} \Omega \cdot m$ [48]). These electrically conductive silver tracks can be used in fabrication of many microelectronic applications such as metallization in printed circuit board (PCB) and radio frequency identification (RFID) tags, collectors for organic light emitting diodes (OLED) and solar cells, and electrodes for thin-film transistor (TFT) circuits etc.



(a)



(b)

Figure 23 (a) linearly Ohmic I –V curve of the printed lines (b) AFM image and cross– sectional profile of a typical silver line printed by multi-nozzle EHD inkjet printing process

5.2 Results of 5ND Multi-Nozzle EHD Inkjet Printing Head

This section presents the printed results of the Multi-nozzle EHD inkjet printing head consisting of five nozzles and having discrete counter electrode (plate). 5ND multi-nozzle EHD inkjet printing head was successfully tested by simultaneously printing electrically conductive lines of copper colloidal solution onto the glass substrate. The details and characterization of the printed results are illustrated in the following subsections.

5.2.1 Axisymmetric Micro-jet Generation

Figure 24 shows high speed camera images of stable meniscus formed at the tip of individual nozzles of 5ND multi-nozzle EHD inkjet print head. Axisymmetric Taylor cone-jets were formed at the tip of each nozzle i.e. nozzle 1, nozzle 2 and nozzle 3, nozzle 4, nozzle 5, whose pinnacle emitted very small jets ($5\pm 1\mu\text{m}$) at an applied dc voltage and flow rate of 2.6 kV and $10\mu\text{l/h}$ respectively. These generated jets were then impinged simultaneously onto a moving substrate, forming electrically conductive micro-tracks of copper nanoparticles.

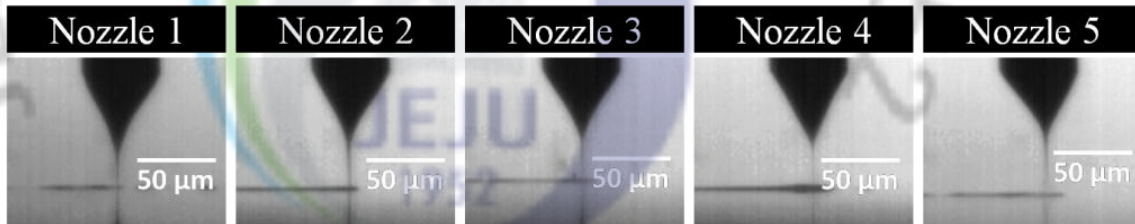


Figure 24 High speed camera images of axisymmetric cone-jets formed at the nozzles tips of 5ND multi-nozzle EHD inkjet print head

5.2.2 Printed Results on Glass Substrate

Figure 25 shows the optical microscope images of continuous copper tracks simultaneously printed by five nozzles onto glass substrate. Since the substrate i.e. glass has a hydrophilic surface therefore, the deposited jets were able to spread out so that the width of the lines became larger than the original size of the generated jets ($5\pm 1\mu\text{m}$). The average line width of the printed tracks is $30\mu\text{m}$ with standard deviation of $2\mu\text{m}$.

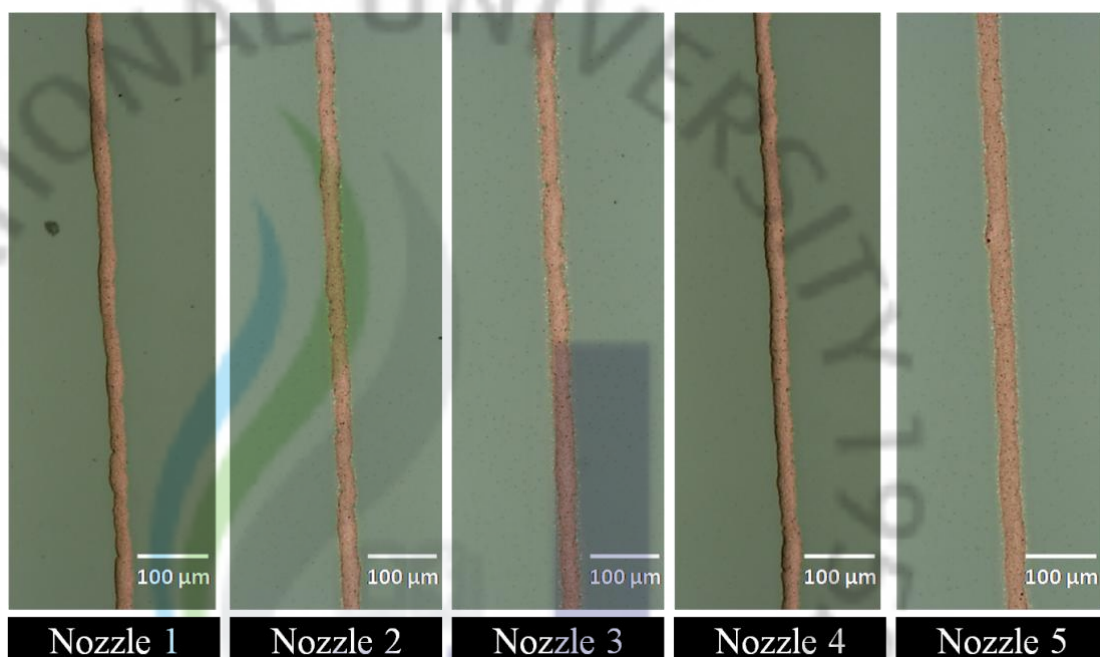


Figure 25 Optical microscope images of continuous copper tracks printed simultaneously onto glass substrate using 5ND multi-nozzle EHD inkjet printing head

5.2.3 X-ray diffraction Analysis of the Printed Lines

Figure 26 shows the XRD spectrum of the deposited copper tracks printed by multi-nozzle EHD inkjet printing technique and sintered at 230°C under inert atmosphere. It is indicated that the three diffraction peaks at $2\theta = 43.26^\circ$, 50.45° and 74.20° attributed to the (111), (200) and (220) planes respectively. Since the phases in Figure 26 show the existence of copper only, therefore it is confirmed that the copper nanoparticles had remained pure during the printing as well as during the sintering process.

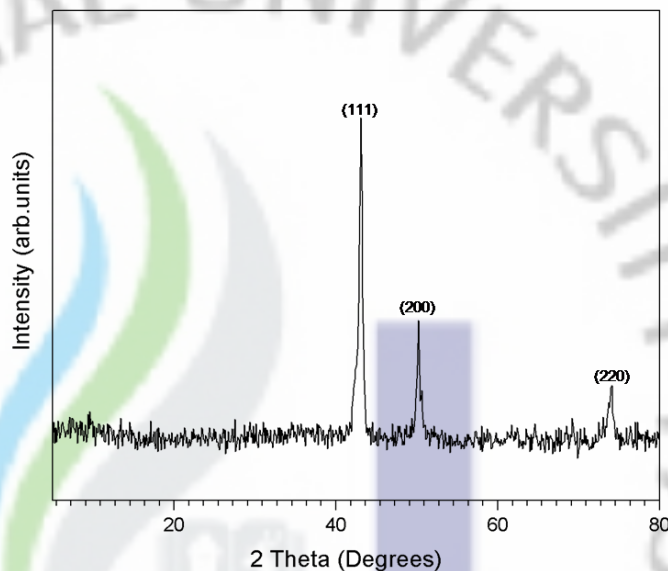


Figure 26 XRD Pattern of the multi-nozzle EHD inkjet Printed copper film, sintered at 230 °C under inert atmosphere

5.2.4 Scanning Electron Microscopy of the Printed Lines

Figure 27 shows the SEM image of a typical copper track printed through 5ND multi-nozzle EHD inkjet printing head. It is evident from the inset of Figure 27 that the nanoparticles are three-dimensionally interconnected with each other however, significant coarsening occurs as the grain grows at the expense of the small particles. Because of this coarsening, the film becomes relatively porous, which may adversely affect the conductivity.

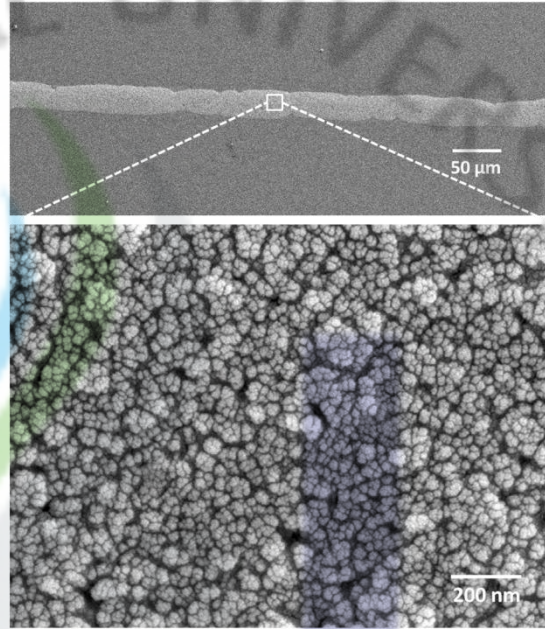
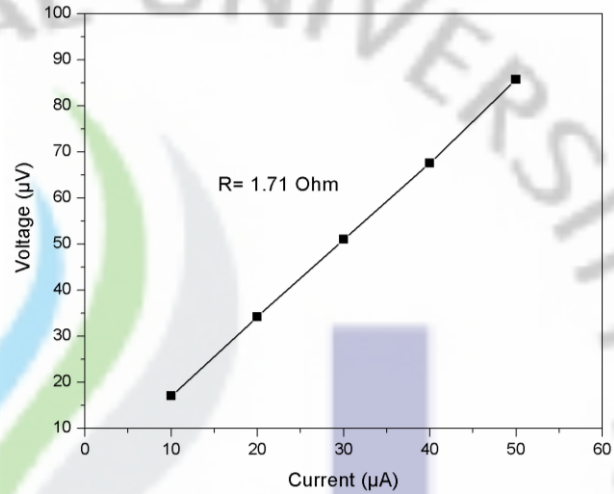


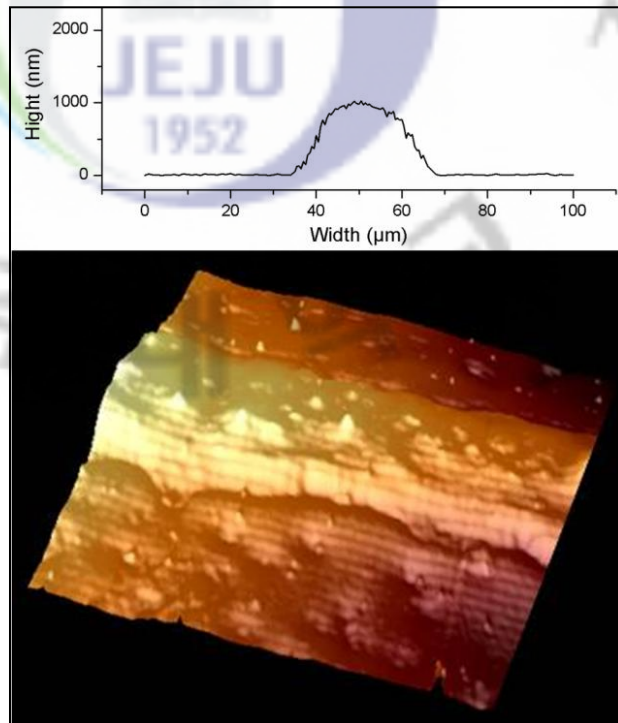
Figure 27 SEM image of copper track deposited by 5ND multi-nozzle EHD inkjet printing head. The bottom inset shows that copper nanoparticles are three-dimensionally interconnected with each other

5.2.5 Electrical Characterization of the Printed Lines

After sintering at 230°C, in inert atmosphere (1atm) for 1h at a constant heating rate of 2°C/min, the resistance R of the printed copper lines was measured by using standard 4-point method. Linearly Ohmic I-V curve (Figure 28a) was obtained by measuring voltage drop ΔV across a 5 mm long sample of printed line by applying current I of different intensity (10μA, 20μA, 30μA, 40μA, 50μA). The electrical resistivity ρ of printed lines were then calculated from the resistance R , the length L , and the cross sectional area A of the line using $\rho = R \cdot A / L$. and cross-sectional area was determined by numerical integration of measured profile from the AFM image of the printed line shown in Figure 28b. The value of resistivity was calculated to be $9.20 \times 10^{-8} \Omega \cdot m$ which is almost five times high as compared to bulk copper resistivity at room temperature ($1.70 \times 10^{-8} \Omega \cdot m$).



(a)



(b)

Figure 28(a) Linearly Ohmic I-V curve of the printed copper conductive lines **(b)** Cross-sectional image and AFM 3D topographical view ($100\ \mu\text{m} \times 100\ \mu\text{m}$) of a typical copper track on a glass substrate, printed by 5ND multi-nozzle EHD inkjet printing head

5.3 Results of 5NI Multi-Nozzle EHD Inkjet Printing Head

This section presents the printed results of the Multi-nozzle EHD inkjet printing head consisting of five nozzles and having integrated counter electrode (ring). 5NI multi-nozzle EHD inkjet printing head was successfully tested by simultaneously printing electrically conductive lines of silver organic ink onto the glass substrate. The details and characterization of the printed results are illustrated in the following subsections.

5.3.1 Printed Results on Glass Substrate

Optimizing the experimental parameters, printing of silver organic ink was performed at an applied dc voltage and flow rate of 3.9 kV and 20 $\mu\text{l/h}$ respectively. **Figure 29** shows the optical microscope images of five continuous silver lines simultaneously printed by 5NI multi-nozzle EHD inkjet printing head onto glass substrate. The average line width of the printed tracks is 140 μm with standard deviation of 5 μm .

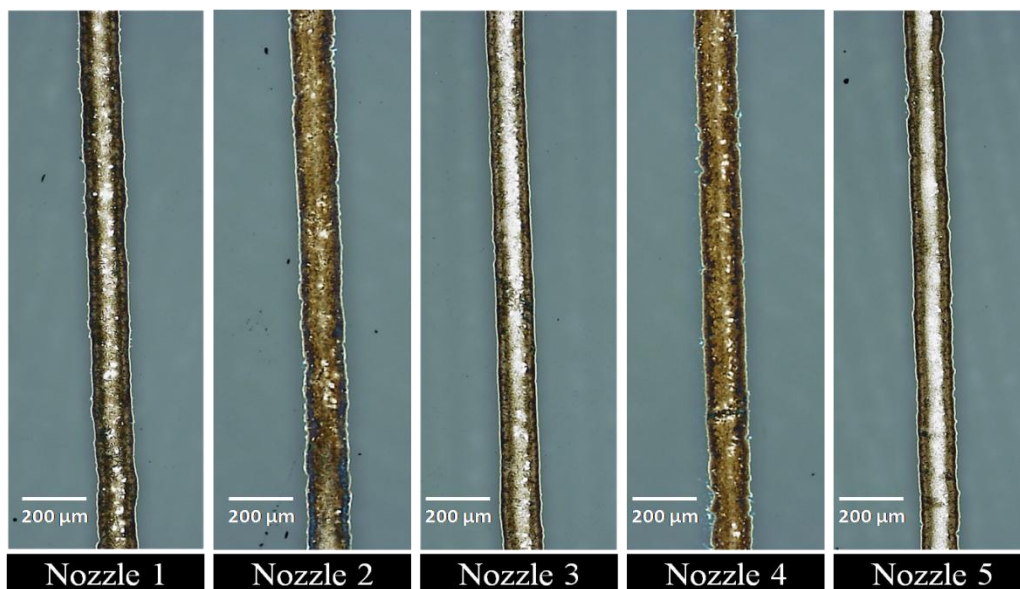


Figure 29 Optical microscope images of continuous silver tracks printed simultaneously onto glass substrate using 5NI multi-nozzle EHD inkjet printing head

5.3.2 Scanning Electron Microscopy of the Printed Lines

The SEM image (Figure 30) shows the microstructure of the printed tracks at various magnification. The SEM image reveals that the surface in the center of the line is consists of densely packed crystallites. Some porosity observed comes from the gaseous byproducts in the ink decomposition during curing. After the gas leaves the system, a metallic silver film with a good electrical conductivity is developed. However, the porosity will inevitably increase the resistivity.

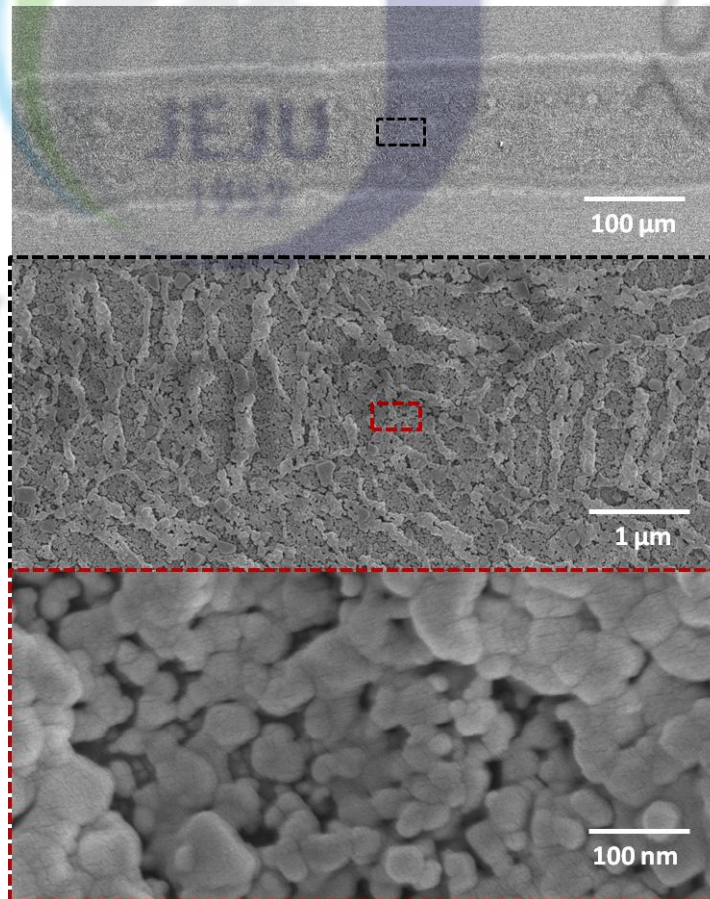


Figure 30 SEM image of silver track deposited by 5NI multi-nozzle EHD inkjet printing head. The bottom insets show densely packed crystallites.

5.3.3 Electrical Characterization of the Printed Lines

After sintering at 250°C for 1h at a constant heating rate of 2°C/min, the resistance R of the printed silver tracks was measured to be $2.60 \times 10^{-3} \Omega$ by using standard 4-point probe (FPP-RS8, Dasol Eng.). The electrical resistivity ρ of printed lines were then calculated from the resistance R , the length L , and the cross sectional area A of the line using $\rho = R \cdot A / L$. The cross-sectional area was determined by numerical integration of measured profile from the AFM image of the printed line shown in Figure 31. The value of resistivity was calculated to be $6.47 \times 10^{-8} \Omega \cdot \text{m}$ which is almost four times high as compared to bulk silver resistivity at room temperature ($1.59 \times 10^{-8} \Omega \cdot \text{m}$).

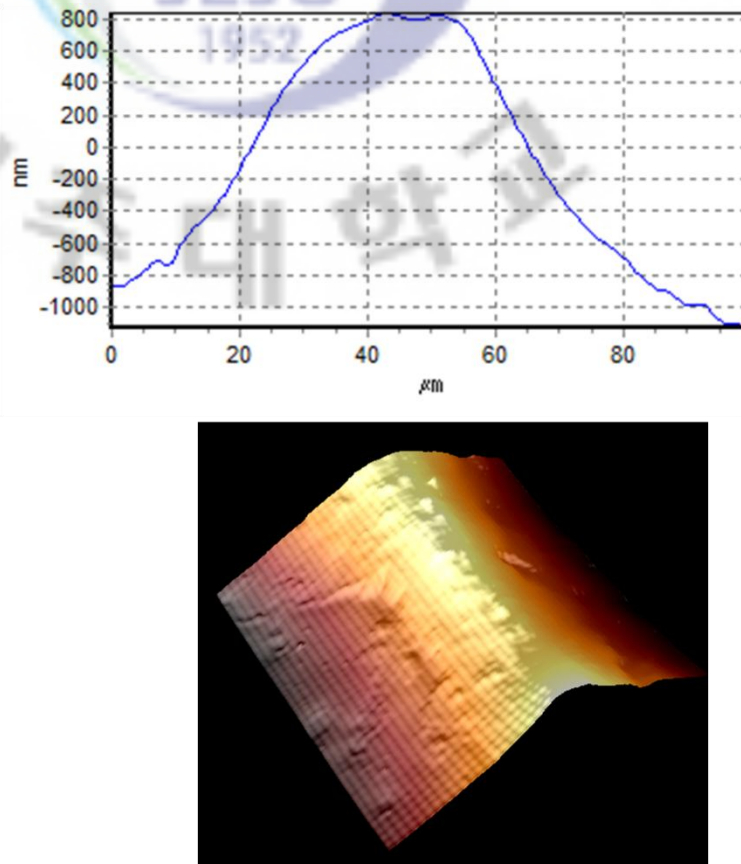


Figure 31 Cross-sectional image and AFM 3D topographical view ($100 \mu\text{m} \times 100 \mu\text{m}$) of a typical silver line on a glass substrate, printed by 5NI multi-nozzle EHD inkjet printing head

Conclusions

To overcome the limitation of low production speed of EHD inkjet printing process and to fabricate low cost electronic microstructures, this thesis presents the investigation and development of multi-nozzle EHD inkjet printing process. First, both numerical and experimental investigations were performed to gain insight understanding of the cross-talk between the neighboring jets. Secondly, based on these investigations a prototype multi-nozzle inkjet printing head (3ND) consisting of three nozzles and having discrete counter electrode was fabricated and tested successfully by optimizing the distance between the nozzles (3mm nozzle-to-nozzle distance). Next, this prototype multi-nozzle EHD inkjet printing head (3ND) has been successfully improved to five nozzles EHD inkjet printing head (5ND), having discrete counter electrode and 2mm nozzle-to-nozzle distance. Lastly, to avoid the cross-talk between the neighboring jets and the effects of substrate on the printing parameters, a novel multi-nozzle inkjet print head (5NI) consisting of five nozzles and having integrated counter electrode has been designed. In this multi-nozzle inkjet print head, substrate effects on printing parameters are eliminated by integrating the ring shaped ground electrodes with each nozzle of the printing head. The printed results of 3ND, 5ND, and 5NI multi-nozzle EHD inkjet printing heads were analyzed both physically and electrically by using different characterization tools such as optical microscopy, scanning electron microscopy (SEM), atomic force microscopy (AFM), X-ray diffraction (XRD) and four-point probe. These electrically conductive micro-tracks demonstrate the feasibility of multi-nozzle EHD inkjet printing process in industrial fabrication of microelectronic structures and devices.

References

1. H. H. Lee, K. S. Chou, K. C. Huang, *Nanotechnology* **16**, 2436 (2005)
2. R. A. Street, W. S. Wong, S. E. Ready, M. L. Chabiny, A. C. Arias, S. Limb, A. Salleo, R. Lujan, *Mater. Today* **9**, 32 (2006)
3. B. J. D. Gans, P. C. Duineveld, U. S. Schubert, *Adv. Mater.* **16**, 203 (2004)
4. M. Einata, N. Einat, *Appl. Phys. Lett.* **89**, 073505 (2006)
5. Y. Wang, J. Bokor, *J. Micro-Nanolith. Mem.* **6**, 043009 (2007)
6. B. H. King, M. J. O'Reilly, S. M. Barnes, *IEEE Conf.*, 001107 (2009)
7. H. F. Poon, *Electrohydrodynamic Printing*. PhD Thesis, Princeton University (2002)
8. J. U. Park, M. Hardy, S. J. Kang, K. Barton, K. Adair, D. K. Mukhopadhyay, C.Y. Lee, M. S. Strano, A. G. Alleyne, J. G. Georgiadis, P. M. Ferreira, J. A. Rogers, *Nat. Mater.* **6**, 782 (2007)
9. R. K. F. Teng, A.A. Mostafa, A. Karim, *IEEE Trans. Indus. Elec.* **37**, 419 (1990)
10. E. Menard, M.A. Meitl, Y. Sun, J.U. Park, D.J.L. Shir, Y.S. Nam, S. Jeon, J.A. Rogers, *Chem. Rev.* **107**, 1117 (2007)
11. S. Khan, Y.H. Doh, A. Khan, A. Rahman, K.H. Choi, D.S. Kim, *Current Appl. Phys.*, doi:10.1016/j.cap.2010.11.044 (2011)
12. Y. Zhouping, H. Yongan, B. Ningbin, W. Xiaomei, X. Youlun, *Chinese Sci. Bull.* **55**, 3383 (2010)
13. S. N. Jayasinghe, M.J. Edirisinghe, *Mater. Res. Innovat.* **7**, 62 (2003)
14. J. S. Lee, Y. S. Kim, Y. J. Kim, *Appl. Phys. Lett.* **93**, 243114 (2008)
15. D. Byun, S. B. Quang Tran, V. D. Nguyen, *J. Electrostatics* **68**, 138 (2010)
16. S. Roy, *J. Phys. D Appl. Phys.* **40**, (2007)

17. A. Jaworek, A.T. Sobczyk, *J. Electrostatic.* **66**, (2008)
18. G. Taylor, Royal Society of London. Series A, Mathematical and Phys. Sci. **280**, (1964)
19. J. U. Park, High-Resolution Electrohydrodynamic Jet Printing Methods For Applications In Electronics and Biotechnology, PhD Thesis, University of Illinois at Urbana-Champaign, (2009)
20. J. L. Li, *J. Electrostatic.* **65**, 251 (2007)
21. A. Jaworek, A. Krupa, *J. Aerosol Sci.* **30**, 673 (1999)
22. D. A. Saville, *Ann. Rev. Fluid Mech.* **29**, 26 (1997)
23. J. K. Nelson, *IEEE Elect. Insulation Mag.* **10**, 16 (1994)
24. L. K. Lim, J. Hua, C.H. Wang, K. A. Smith, *AIChE Journal* **57**, 57 (2011)
25. A. Ganan-Calvo, M. J. Davila, A. Barrero, *J. Aerosol Sci.* **28**, 249 (1997)
26. D. P. H. Smith, *IEE transaction of Industry Applications*, 527 (1986)
27. M. Cloupeau, B. Prunetfoch, *J. Aerosol Sci.* **25**, 1021 (1994)
28. M. Cloupeau, B. Prunetfoch, *J. Electrostatic.* **23**, 165 (1990)
29. J. L. Li, P. Zhang, *J. Electrostatic.* **67**, 562 (2009)
30. S. Umezu, R. Nakazawa, H. Kawamo, Cross-Talk of Multi-Nozzle in Electrostatic Inkjet System, International Conference on Digital Printing Technologies, 66-68 (2008)
31. A. J. Rulison, R.C. Flagan, *Rev. Sci. Instrum.* **64**, 683 (1993)
32. T. H. J. Osch, J. Perelaer, A. W. M. Delaat, U.S. Schubert, *Adv. Mater.* **20**, 343 (2008)
33. D.Y. Lee, Y.S. Shin, S.E. Park, T.U. Yu, J. Hwang, *Appl. Phys. Lett.* **90**, 081905 (2007)
34. K. Wang, J. P.W. Stark, *Appl. Phys. A* **99**, 763 (2010)
35. J. H. Yu, S. Y. Kim, J. Hwang, *Appl. Phys. A* **89**, 157 (2007)
36. K. Wang, M. D. Paine, J. P. W. Stark, *Appl. Phys. Lett.* **106**, 024907 (2009)

37. D.H. Youn, S.H. Kim, Y.S. Yang, S.C. Lim, S.J. Kim, S.H. Ahn, H.S. Sim, S.M. Ryu, D.W. Shin, J.B. Yoo, *Appl. Phys. A* **96**, 933 (2009)
38. C.M. Hong, S. Wanger, *IEEE Electron Devise Lett.* **21**, 384 (2000)
39. B. K. Park, D. Kim, S. Jeong, J. Moon, J. S. Kim, *Thin Solid Films* **515**, 7706 (2007)
40. Y. Lee, J. R. Choi, K. J. Lee, N.E. Stott, D. Kim, *Nanotech.* **19**, 1 (2008)
41. J. S. Kang, H. S. Kim, J. Ryu, H.T. Hahn, S. Jang, J. W. Joung, *J Mater. Sci: Mater Electron.* **21**, 1213 (2010)
42. K.C. Yung, T.S. Plura, *Appl. Phys. A* **101**, 393 (2010)
43. D. S. Kim, A. Khan, K. Rahman, S. Khan, H.C. Kim, K.H. Choi, *Mater. Manuf. Proc.* DOI: 10.1080/10426914.2011.551956 (2011)
44. B. Q. T. Si, D. Byun, S. Lee, *J. Aerosol Sci.* **38**, 924 (2007)
45. V. Subramanian, J. M. J. Frechet, P. C. Chang, D.C. Huang, J. B. Lee, S.E. Molesa, A.R. Murphy, D.R. Redinger, S.K. Volkman, *IEEE Proc.* **93**, 1330 (2005)
46. J. Choi, Y. J. Kim, S. Lee, S. U. Son, H. S. Ko, V. D. Nguyen, D. Byun, *Appl. Phys. Lett.* **93**, 193508 (2008)
47. R.D. Deegan, O. Bakajin, T.F. Dupont, G. Huber, S.R. Nagel, T.A. Witten, *Nat.* **389**, 827 (1997).
48. S. B. Fuller, E. J. Wilhelm, J. M. Jacobson, *J. Microelectromech. Syst.* **11**, 54 (2002)

List of Publications

Journal Publications

- **A. Khan**, K. Rahman, M. T. Hyun, D. S. Kim, and Kyung Hyun Choi, Multi-nozzle electrohydrodynamic inkjet printing of silver colloidal solution for the Fabrication of Electrically Functional Microstructures, *Applied Physics A: Materials Science and Processing*, DOI: 10.1007/s00339-011-6386-0 (in press)
- K. H. Choi, **A. Khan**, K. Rahman, Y. H. Doh, D.S. Kim and K.R. Kwan, Effects of nozzles array configuration on cross-talk in multi-nozzle electrohydrodynamic inkjet printing head, *Journal of Electrostatics*, DOI: 10.1016/j.elstat.2011.04.017 (in press)
- D. S. Kim, **A. Khan**, K. Rahman, S. Khan, H. C. Kim, and K. H. Choi, Drop-on-demand direct printing of colloidal copper nanoparticles by electrohydrodynamic atomization, *Materials and Manufacturing Processes*, DOI: 10.1080/10426914.2011.551956 (in press)
- **A. Khan**, K. Rahman, K. H. Choi and D. S. Kim, direct writing of copper conductive micro-tracks by multi-nozzle electrohydrodynamic inkjet printing process, *Journal of Materials Processing Technology* (Under Review)
- S. Khan, Y. H. Doh, **A. Khan**, A. Rahman, K. H. Choi, and D. S. Kim, Direct patterning and electrospray deposition through EHD for fabrication of printed thin Film transistors, *Current Applied Physics*, Vol. 11, No: 01, pp. S271-S279 (2011)
- K. Rahman, **A. Khan**, N. M. Nam, K. H. Choi, and D. S. Kim, Study of electrohydrodynamic drop-on-demand printing through multi-step pulse voltage, *International Journal of Precision Engineering and Manufacturing*, Vol. 12 / No. 4 (to be published in August, 2011)

- K. H. Choi, A. Ali, A. Rahman, N.M. Malik, K. Rahman, **A. Khan**, S. Khan and D. S. Kim, Electrode configuration effects on electrification and voltage variation in electrostatic inkjet printing head, *Journal of Micromechanics and Microengineering*, Vol. 20 / No.7, pp. 075033 (2010)
- A. Ali, A. Rahman, K. Rahman, N.M. Malik, **A. Khan**, S. Khan, J. B. Ko, B. S. Yang, H. C. Kim, Y. H. Doh, D. S. Kim and K. H. Choi, Printed patterns adhesion dependency on contact angle of ink on substrate, *International Journal of Engineering & Technology*, Vol. 10 / No. 01, pp. 95-100 (2010)

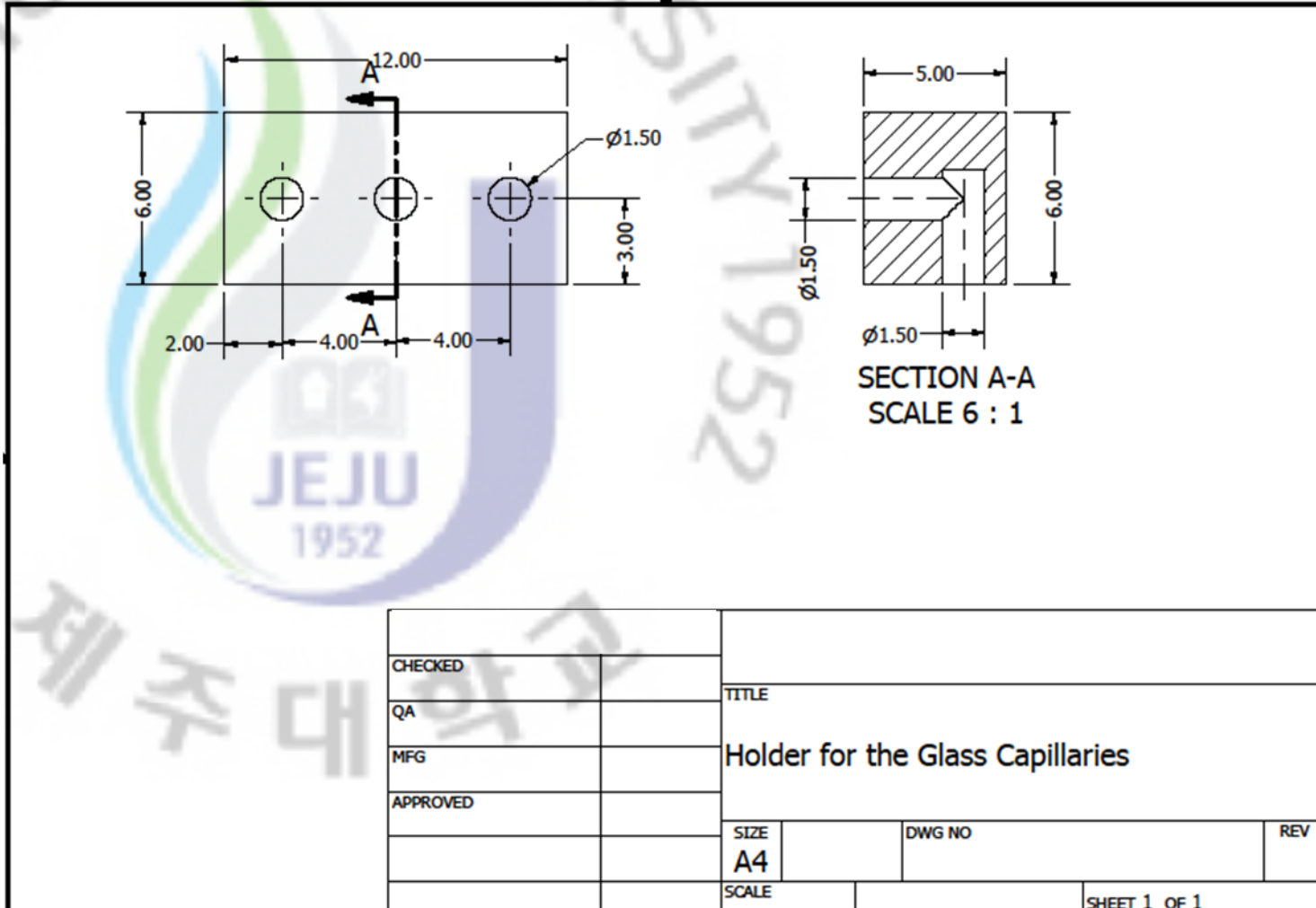
International Conferences and Workshops

- **A. Khan**, K. Rahman, H. C. Kim, K. H. Choi and D. S. Kim, Effects of process parameters on cross-talk in triangular array multi-nozzle EHD inkjet printing head, *Proc. of IEEE-ICIET 2010*, DOI:10.1109/ICIET.2010.5625704
- **A. Khan**, K. Rahman, K. H. Choi and D. S. Kim, Multi-nozzle EHD jetting of conductive colloidal ink, *Proc. of KSME, April 22-23, 2010, Jeju Island, South Korea*, pp.346-348
- K. Rahman, **A. Khan**, N. M. Nam, K. H. Choi and D. S. Kim, Study of electrohydrodynamic drop-on-demand printing through multi-step pulse voltage, *Proc. of 7th International Workshop on Microfactories*, October 24-27, 2010, Daejeon, South Korea, pp.203-208
- A. Ali, A. Rahman, **A. Khan**, K. H. Choi, S. Khan and D. S. Kim, Development and analysis of EHD inkjet printing head by introducing ring shaped electrode, *Proc. of KSME, April 22-23, 2010, Jeju Island, South Korea*, pp.194-197



Appendices

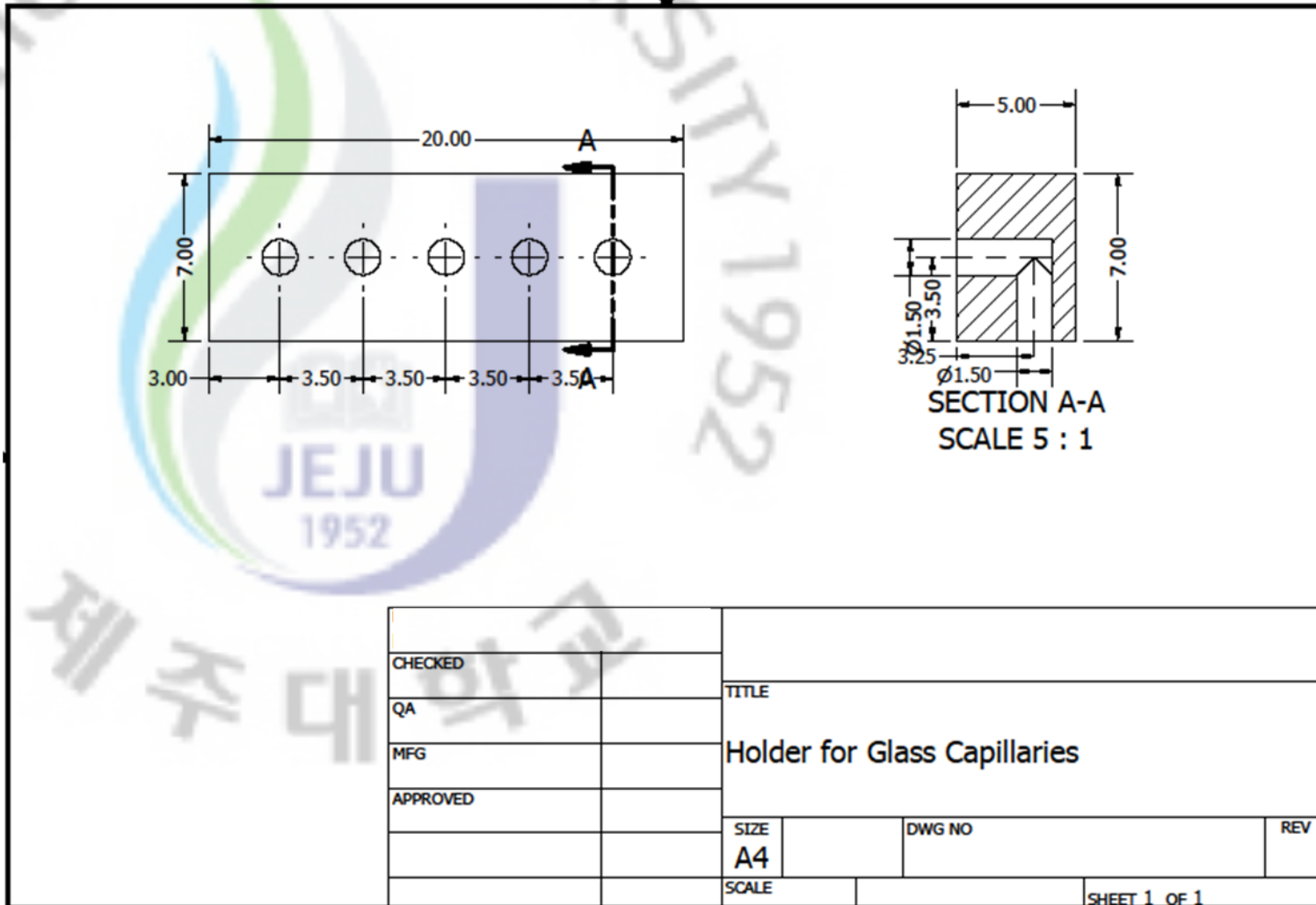
APPENDIX A



CHECKED		TITLE	
QA		Holder for the Glass Capillaries	
MFG		SIZE	DWG NO
APPROVED		A4	REV
		SCALE	SHEET 1 OF 1

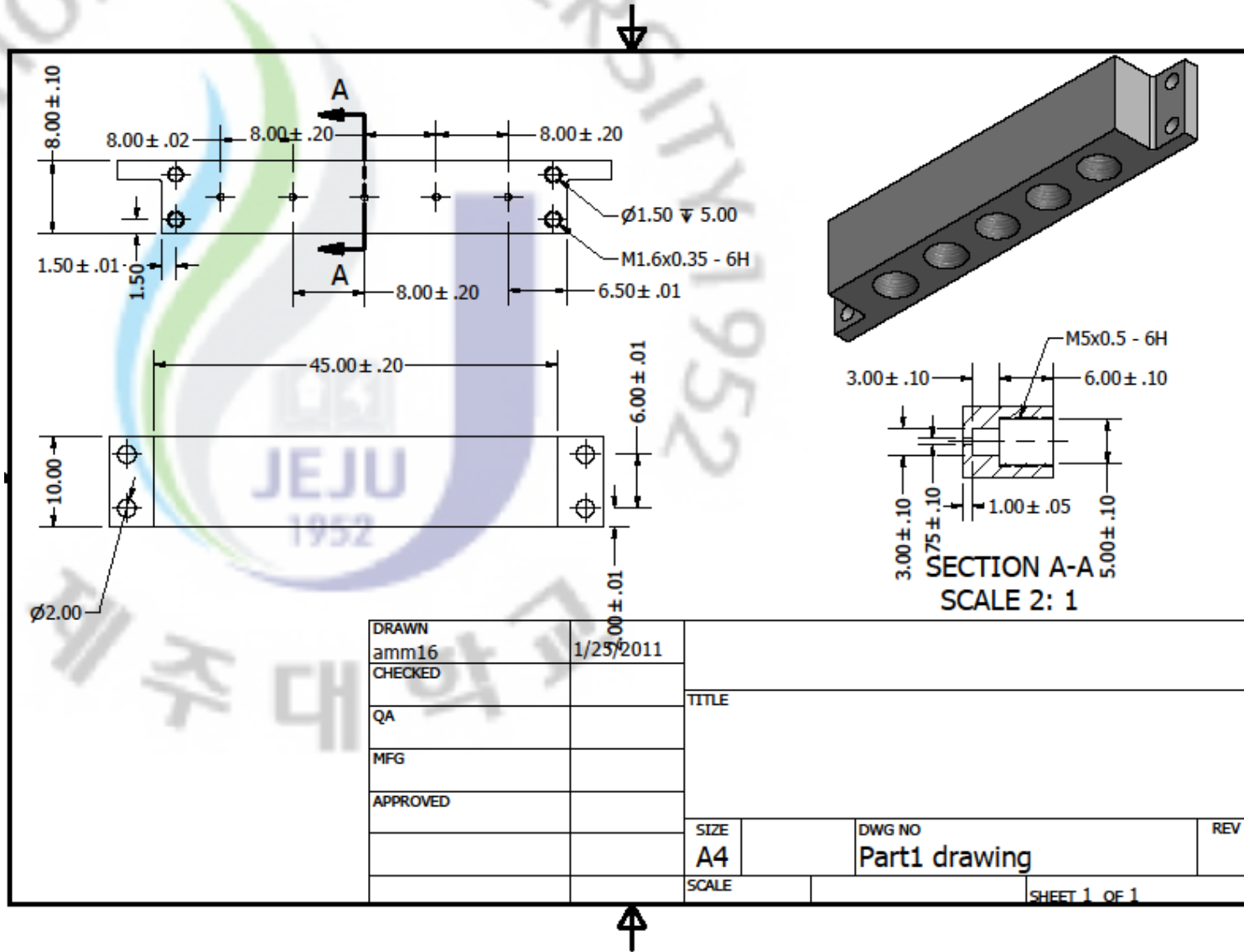


APPENDIX B

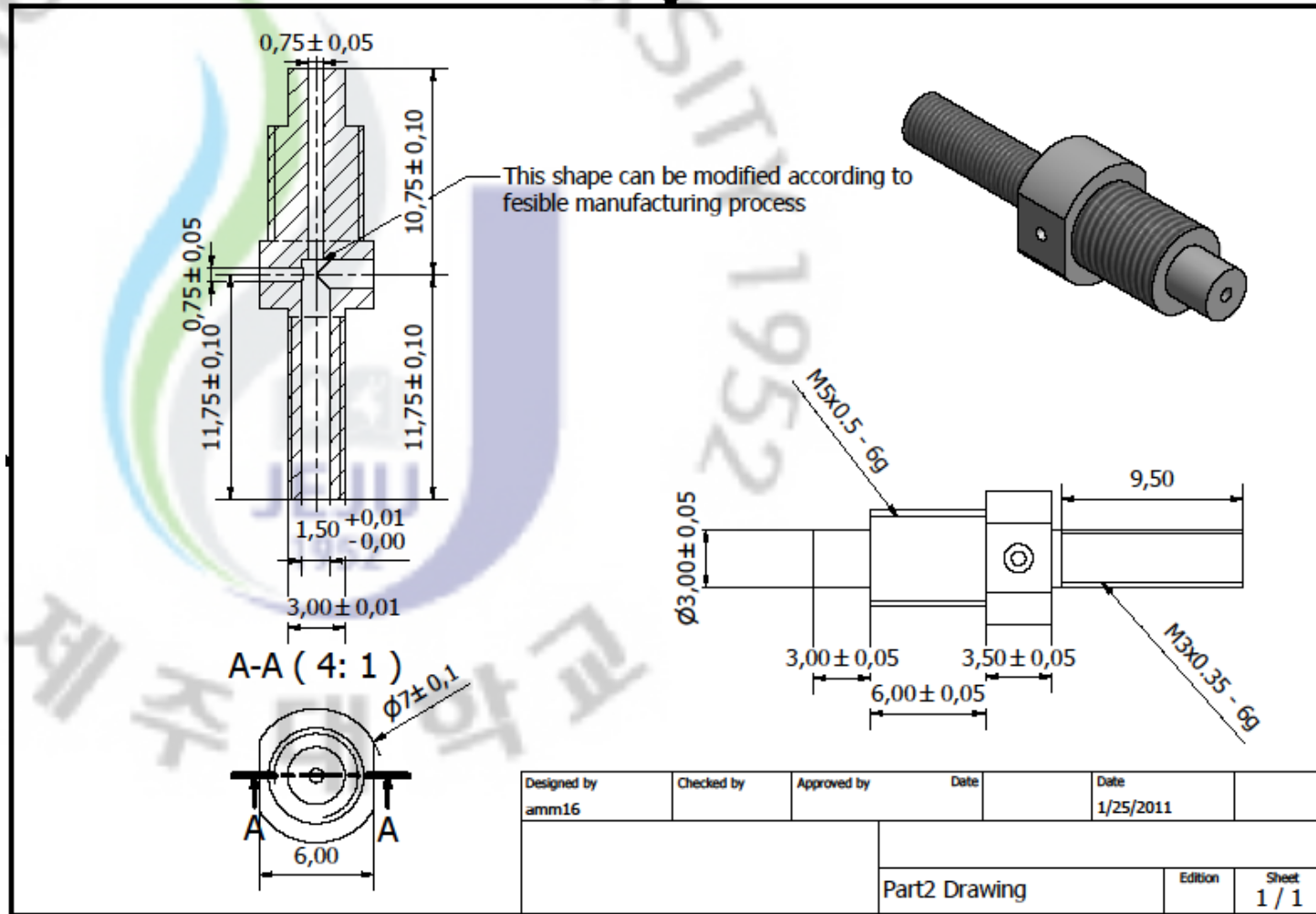


CHECKED		TITLE	
QA		Holder for Glass Capillaries	
MFG		SIZE	DWG NO
APPROVED		A4	REV
		SCALE	SHEET 1 OF 1

APPENDIX C1

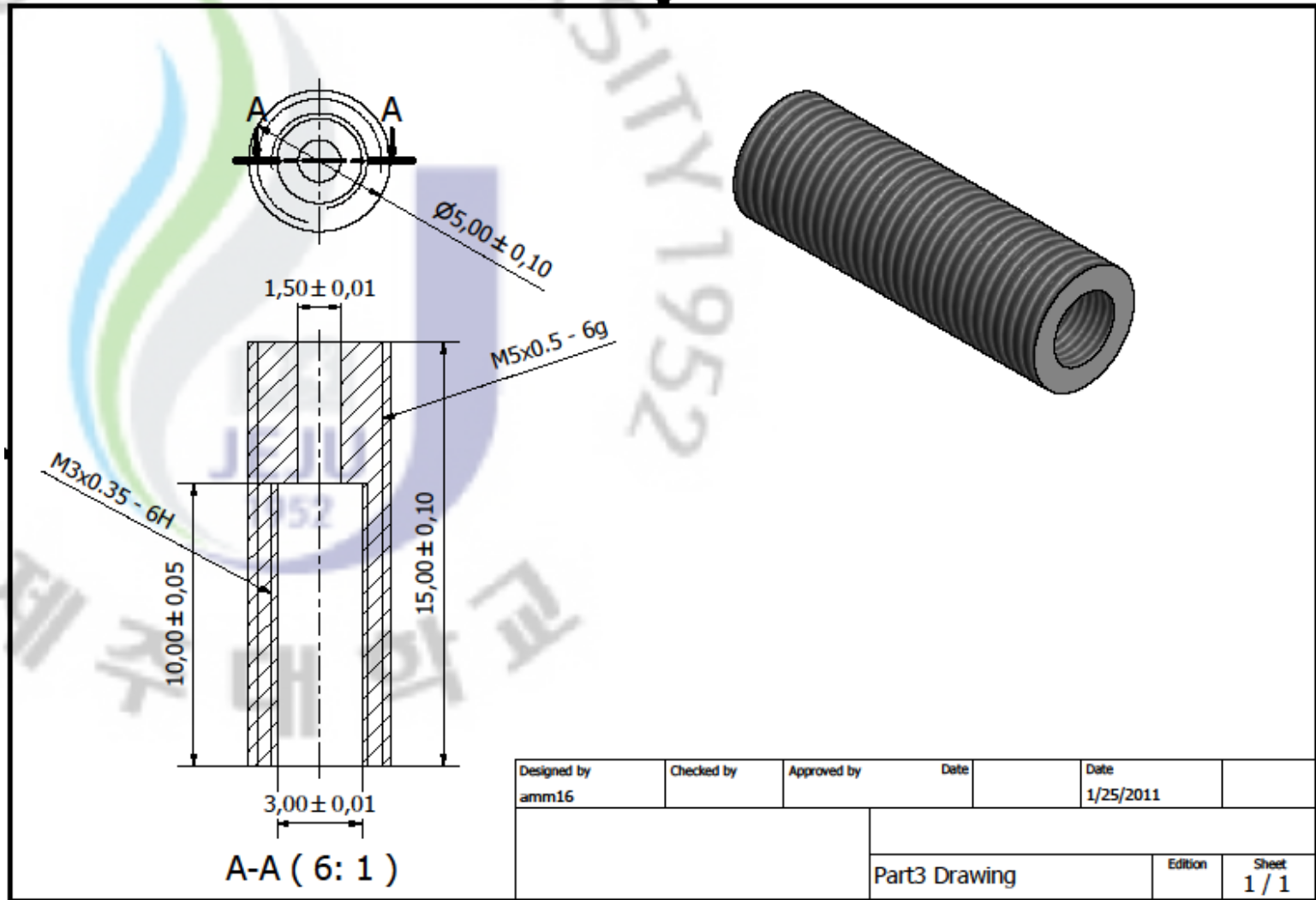


APPENDIX C2

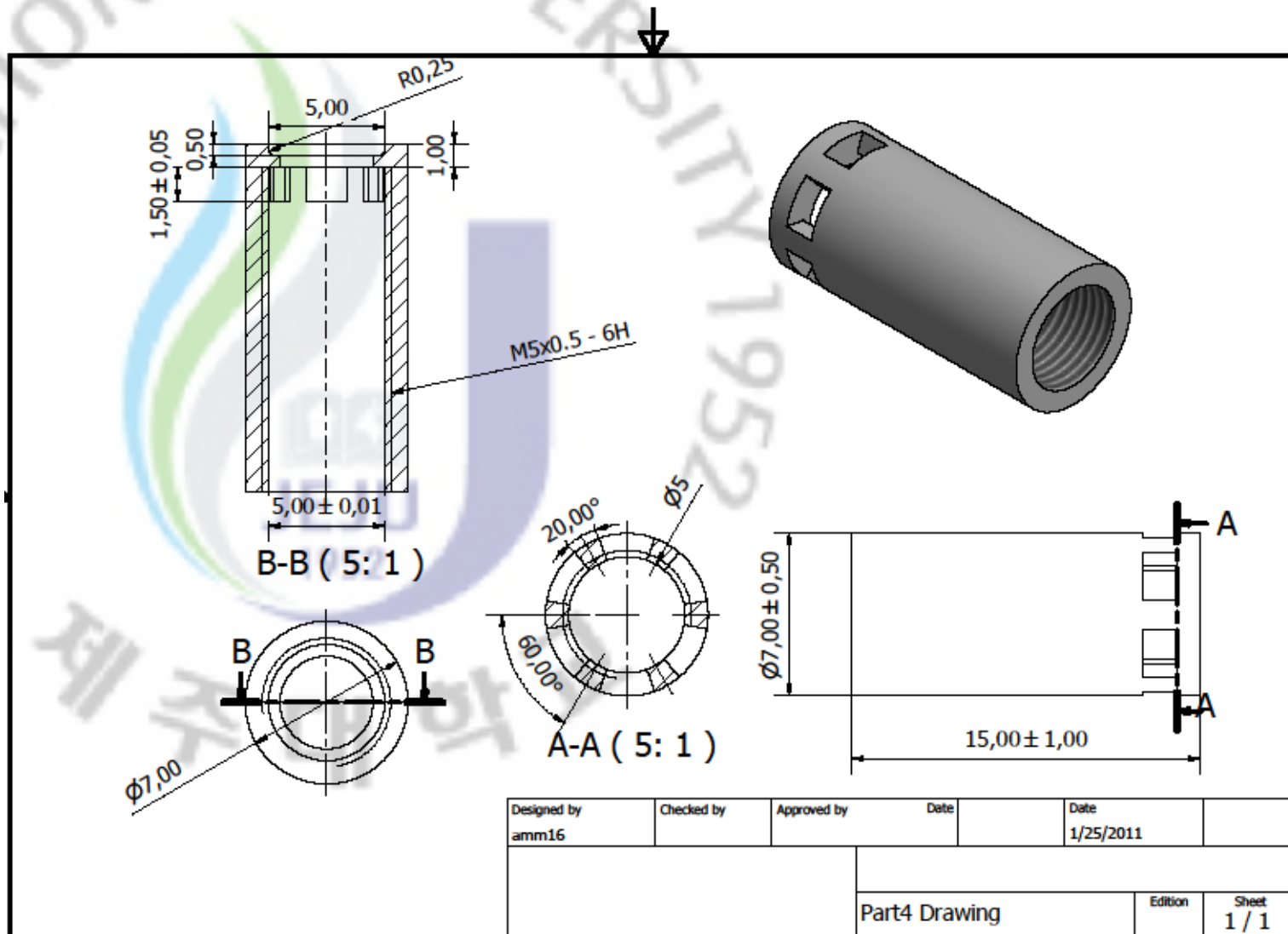


Designed by amm16	Checked by	Approved by	Date	Date 1/25/2011	
			Part2 Drawing		Edition
					Sheet 1 / 1

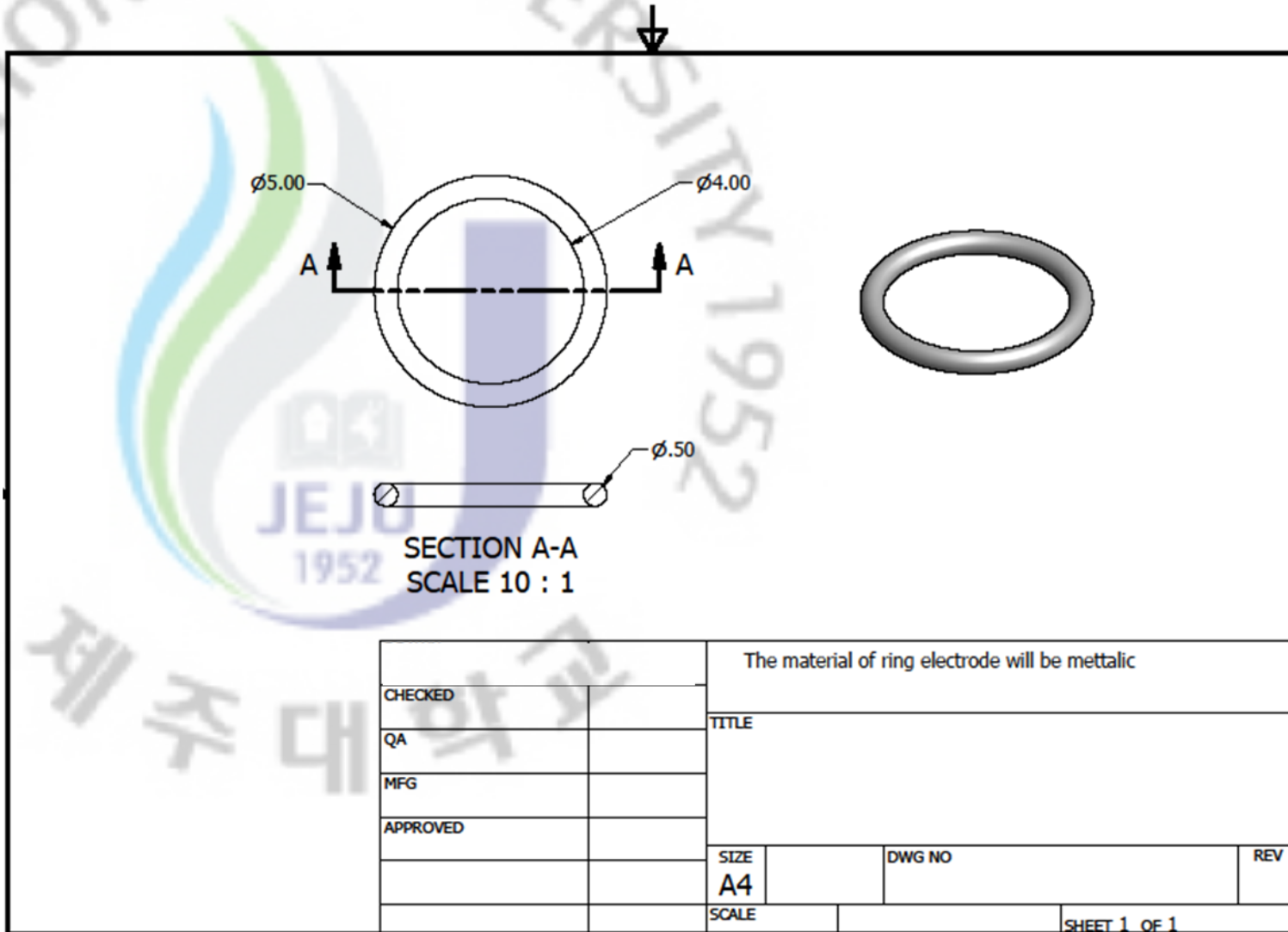
APPENDIX C3



APPENDIX C4



APPENDIX C5



		The material of ring electrode will be mettalic		
CHECKED		TITLE		
QA				
MFG				
APPROVED				
		SIZE	DWG NO	REV
		A4		
		SCALE		SHEET 1 OF 1